Hypersingular integral and integro-differential micromechanical models for an imperfect interface between a thin orthotropic layer and an orthotropic half-space under inplane elastostatic deformations*

Xue Wang, Whye-Teong Ang+ and Hui Fan
School of Mechanical and Aerospace Engineering
Nanyang Technological University
Singapore 639798

Abstract

Micromechanical models are proposed here for estimating the effective stiffness coefficients of a micro-cracked interface between a thin orthotropic layer and an orthotropic half-space under inplane elastostatic deformations. The micromechanical models are formulated and numerically solved in terms of hypersingular integral and integro-differential equations. Specific case studies involving particular orthotropic materials and isotropic materials are conducted to gain insights into the macroscopic behaviors of the interface.

Keywords: Micromechanics, imperfect interface, effective stiffness coefficients, thin film, hypersingular integral and integro-differential equations.

* This is a preprint of a paper published in:
Engineering Analysis with Boundary Elements 52 (2015) 32-43.
+ Author for correspondence

1 Introduction

Thin film structures are nowadays widely used in many engineering applications, such as in microelectronics. They may be formed by coating a layer of material on a substrate of dissimilar material at a very high temperature. During the manufacturing process, the elastic or thermal mismatch between the thin film and the substrate may induce severe residual stresses, giving rise to the formation of interfacial micro-defects.

A microscopically damaged interface may be modeled as containing a distribution of micro-cracks. At the macro level, the micro-cracked interface may be regarded as a spring-like imperfect interface characterized by a set of stiffness coefficients. In the macroscopic spring interface model, the displacement field is discontinuous across the interface and the tractions on the interface are linear combinations of the displacement jumps across the interface, as in Hashin [11], Jones and Whittier [13], Martin [15] and Sudak and Wang [20].

A micromechanical problem of interest is the estimation of the effective stiffness coefficients of the spring-like interface. The finite element method based three-phase model in Fan and Sze [8], which simplifies the micro-cracked interface to a single (typical) micro-crack interacting with spring-like (effective) regions having a priori unknown interfacial properties, may be employed to estimate the effective stiffness. Although the three-phase model provides some useful insights into the properties of the spring-like interface, it has a limited applicability, as it does not take into account microscopic details such as the lengths and the positions of the individual interfacial micro-cracks.

In Wang *et al* [21], a microscopically damaged interface subject to an antiplane deformation is modeled using a randomly generated array of inter-

facial micro-cracks that are periodically distributed on the interface. Specifically, a period interval of the interface contains an arbitrary number of randomly positioned micro-cracks with lengths that follow a normal distribution. To estimate the effective stiffness of the antiplane spring-like interface, the micromechanical-statistical model is formulated and solved in terms of a system of hypersingular integral equations. The analysis in [21] is used in Wang *et al* [22] to study the effective stiffness of the interface for more realistic cases where the lengths of the micro-cracks are generated using a chi-square (χ^2) distribution of a low degree of freedom.

The micromechanical-statistical model is employed here to investigate a microscopically damaged interface between an orthotropic thin elastic layer and a dissimilar orthotropic elastic half-space under static inplane deformations. A three-phase model of the interface is also proposed here, mainly for the purpose of verifying the micromechanical-statistical model. The mathematical formulations of both models for inplane deformations are much more involved than those for the corresponding antiplane models in [21] and [22], giving rise to hypersingular integral and integro-differential equations, where the displacement jumps over the imperfect parts of the interface are unknown functions to be determined. Numerical procedures for solving the hypersingular integral and integro-differential equations and estimating the effective stiffness coefficients of the interface are outlined. Specific case studies on the effective stiffness coefficients of the interface are conducted using the models with particular elastic materials in the layer and the half-space. For the case where both materials are isotropic, the coefficients of the hypersingular integral and integro-differential equations in the micromechanical-statistical model are reduced to the Dundurs' parameters of the isotropic bimaterial.

The micromechanical models here are formulated using the differentiated

form of the direct boundary integral equations for elasticity. An advantage of such formulation is that the unknown functions are physically meaningful. For details of the direct boundary integral equations and hypersingular integral equations in elasticity, one may refer to Ang [1], Chen and Hong [4], Clements [6], Hong and Chen [12] and Rizzo [16].

2 The micromechanical interface problem

Consider an infinitely long elastic layer bonded to an elastic half-space. With reference to a Cartesian coordinate frame $Ox_1x_2x_3$, the layer occupies the region $0 < x_2 < h$ (where h is a given positive constant) and the elastic half-space $x_2 < 0$. The materials in the layer and the half-space are orthotropic, having possibly dissimilar properties. At the microscopic level, the interface between the layer and the half space is damaged containing interfacial microcracks with geometries that do not vary along the x_3 direction.

The bimaterial undergoes a plane elastostatic deformation such that the only non-zero components of the Cartesian displacement are u_1 and u_2 and are functions of only x_1 and x_2. The relevant non-zero components of the Cartesian stress σ_{kj} are given by

$$\begin{aligned} \sigma_{11} &= C_{11}(x_2)\frac{\partial u_1}{\partial x_1} + C_{12}(x_2)\frac{\partial u_2}{\partial x_2}, \\ \sigma_{22} &= C_{12}(x_2)\frac{\partial u_1}{\partial x_1} + C_{22}(x_2)\frac{\partial u_2}{\partial x_2}, \\ \sigma_{12} &= \sigma_{21} = C_{66}(x_2)(\frac{\partial u_1}{\partial x_2} + \frac{\partial u_2}{\partial x_1}), \end{aligned} \tag{1}$$

where $C_{11}(x_2)$, $C_{22}(x_2)$, $C_{12}(x_2)$ and $C_{66}(x_2)$ are elastic moduli of orthotropic

materials defined by

$$\begin{aligned}
&(C_{11}(x_2), C_{22}(x_2), C_{12}(x_2), C_{66}(x_2)) \\
&= \begin{cases} (C_{11}^{(1)}, C_{22}^{(1)}, C_{12}^{(1)}, C_{66}^{(1)}) & \text{for } 0 < x_2 < h, \\ (C_{11}^{(2)}, C_{22}^{(2)}, C_{12}^{(2)}, C_{66}^{(2)}) & \text{for } x_2 < 0, \end{cases}
\end{aligned} \tag{2}$$

with $C_{11}^{(p)}, C_{22}^{(p)}, C_{12}^{(p)}$ and $C_{66}^{(p)}$ being positive constants such that

$$\begin{aligned}
&C_{11}^{(p)}\xi_1^2 + C_{22}^{(p)}\xi_2^2 + 2C_{12}^{(p)}\xi_1\xi_2 + C_{66}^{(p)}\xi_3^2 > 0 \\
&\text{for all real numbers } \xi_1,\ \xi_2 \text{ and } \xi_3 \text{ such that } \xi_1^2 + \xi_2^2 + \xi_3^2 \neq 0.
\end{aligned} \tag{3}$$

Note that (3) implies that the strain energy density of the elastic system is strictly positive (see Clements [6] and Eshelby *et al* [7]).

From (1) and the equilibrium equations of plane elastostatics, u_1 and u_2 are required to satisfy the elliptic system of partial differential equations

$$\begin{aligned}
C_{11}\frac{\partial^2 u_1}{\partial x_1^2} + (C_{12} + C_{66})\frac{\partial^2 u_2}{\partial x_1 \partial x_2} + C_{66}\frac{\partial^2 u_1}{\partial x_2^2} &= 0, \\
C_{66}\frac{\partial^2 u_2}{\partial x_1^2} + (C_{12} + C_{66})\frac{\partial^2 u_1}{\partial x_1 \partial x_2} + C_{22}\frac{\partial^2 u_2}{\partial x_2^2} &= 0.
\end{aligned} \tag{4}$$

Details on the elliptic system in (4) may be found in Clements [6].

The displacements u_k and the stresses σ_{kj} along a macroscopic portion of the microscopically damaged interface $x_2 = 0$ may be homogenized by using the averaging procedure

$$\begin{aligned}
\widehat{u}_k(\widehat{x}_1, 0^{\pm}) &= \frac{1}{2\ell}\int_{\widehat{x}_1 - \ell}^{\widehat{x}_1 + \ell} u_k(x_1, 0^{\pm})\, dx_1, \\
\widehat{\sigma}_{kj}(\widehat{x}_1, 0^{\pm}) &= \frac{1}{2\ell}\int_{\widehat{x}_1 - \ell}^{\widehat{x}_1 + \ell} \sigma_{kj}(x_1, 0^{\pm})\, dx_1,
\end{aligned} \tag{5}$$

where $\widehat{x}_1$ and ℓ are the midpoint and the half-length of the macroscopic portion.

The interfacial conditions in the macro-level spring model for the microscopically damaged interface are given by

$$\begin{aligned} \widehat{k}_1 \Delta \widehat{u}_1(\widehat{x}_1) &= \widehat{\sigma}_{12}(\widehat{x}_1, 0^+) = \widehat{\sigma}_{12}(\widehat{x}_1, 0^-), \\ \widehat{k}_2 \Delta \widehat{u}_2(\widehat{x}_1) &= \widehat{\sigma}_{22}(\widehat{x}_1, 0^+) = \widehat{\sigma}_{22}(\widehat{x}_1, 0^-), \end{aligned} \tag{6}$$

where $\Delta \widehat{u}_i(\widehat{x}_1) = \widehat{u}_i(\widehat{x}_1, 0^+) - \widehat{u}_i(\widehat{x}_1, 0^-)$ and $\widehat{k}_1$ and $\widehat{k}_2$ are the effective stiffness coefficients of the interface (see, for example, Hashin [11], Jones and Whittier [13], Martin [15] and Sudak and Wang [20]).

For the macro-level spring model defined by (6) to be valid, the external tensile load acting on the bimaterial along the x_2 direction is assumed to be sufficiently large (dominant) to ensure that $\Delta \widehat{u}_2 > 0$ on the interface.

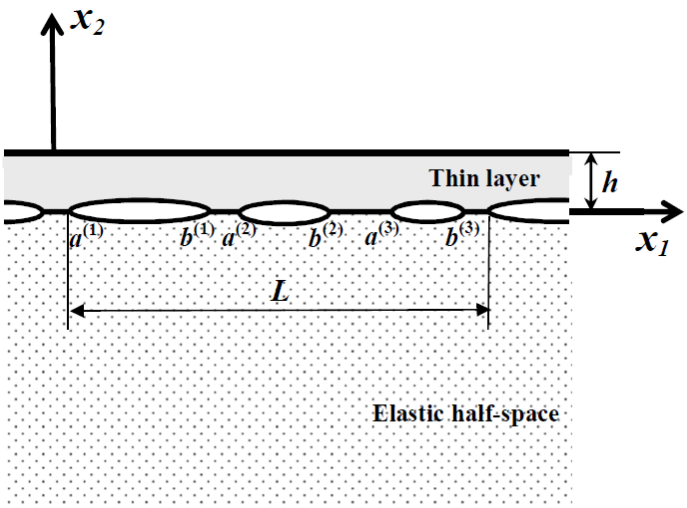

Figure 1. A sketch of the micro-cracked interface containing three micro-cracks over a period interval of the interface. The length of a period interval of the interface is L.

The interface is assumed to be homogeneously damaged at the macro level so that $\widehat{k}_1$ and $\widehat{k}_2$ are constants. At the micro level, such an interface is modeled as containing periodic arrays of micro-cracks. More precisely, M arbitrarily located interfacial micro-cracks of possibly different lengths lie on $0 < x_1 < L$, $x_2 = 0$. The tips of a typical m-th micro-crack on $0 < x_1 < L$, $x_2 = 0$, are given by $(a^{(m)}, 0)$ and $(b^{(m)}, 0)$, where $a^{(m)}$ and $b^{(m)}$ are constants such that $0 < a^{(1)} < b^{(1)} < a^{(2)} < b^{(2)} < \cdots < a^{(M)} < b^{(M)} < L$. The remaining parts of the interface contain micro-cracks defined by $a^{(m)} + nL < x_1 < b^{(m)} + nL$ for $m = 1, 2, \cdots, M$ and $n = \pm 1, \pm 2, \cdots$, that is, the remaining micro-cracks are periodically distributed exact replicas of the M micro-cracks on the interval $0 < x_1 < L$, $x_2 = 0$. A sketch of the micro-cracked interface is given in Figure 1 for $M = 3$.

The problem of interest here is to estimate the effective stiffness coefficients $\widehat{k}_1$ and $\widehat{k}_2$ by taking into consideration some microscopic details of the interface. Two micromechanical models of the interface − the three-phase model and the micromechanical-statistical model − are proposed here for estimating $\widehat{k}_1$ and $\widehat{k}_2$.

3 Three-phase model

3.1 Boundary value problem

The three-phase model here simplifies the period interval $0 < x_1 < L$ of the micro-cracked interface in Figure 1 to three distinct parts:

(a) a single representative micro-crack in the region $c^{(1)} < x_1 < d^{(1)}$, $x_2 = 0$,

(b) perfectly bonded portions in the regions $0 < x_1 < c^{(1)}$ and $d^{(1)} < x_1 < c^{(2)}$ on $x_2 = 0$, and

(c) an effective region $c^{(2)} < x_1 < d^{(2)}$, $x_2 = 0$, where the behaviors of the interface are described by the macro-level spring model with yet to be determined stiffness coefficients $\widehat{k}_1$ and $\widehat{k}_2$.

Note that $c^{(1)}$, $c^{(2)}$, $d^{(1)}$ and $d^{(2)}$ are constants such that $0 < c^{(1)} < d^{(1)} < c^{(2)} < d^{(2)} = L$ and $c^{(1)} = c^{(2)} - d^{(1)}$ and $c^{(2)}$ is small compared to L. The geometry of the entire interface in the three-phase model is periodic with period L. For a sketch of the three-phase model, refer to Figure 2.

The damage ratio ρ defined by

$$\rho = \frac{d^{(1)} - c^{(1)}}{c^{(2)}} \tag{7}$$

gives the fraction of the interface in Figure 1 that are damaged by micro-cracks.

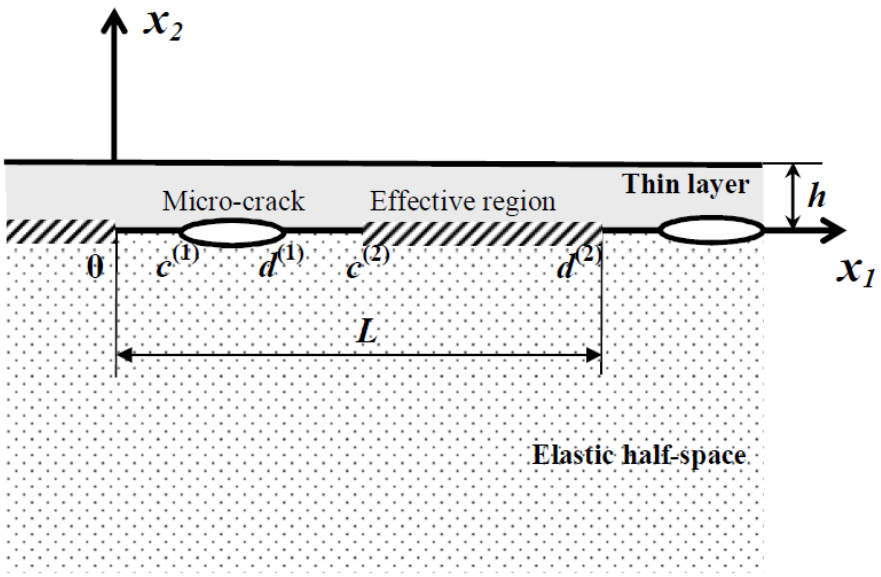

Figure 2. A sketch of the three-phase model.

The three-phase model above is based on the generalized self-consistent scheme proposed by Christensen and Lo [5]. In such a scheme, it is necessary to incorporate the interaction between a simplified microstructure and an effective region with an unknown property. The simplified microstructure here is the micro-cracked region $0 < x_1 < c^{(2)}$, $x_2 = 0$.

The interfacial conditions for the three-phase model are

$$\begin{array}{l} \sigma_{r2}(x_1, 0^{\pm}) = 0 \text{ for } (x_1, 0) \in I_{\text{cracked}}, \\ \left.\begin{array}{rcl} \Delta u_r(x_1) & = & 0 \\ \sigma_{r2}(x_1, 0^+) & = & \sigma_{r2}(x_1, 0^-) \end{array}\right\} \text{ for } (x_1, 0) \in I_{\text{perfect}}, \\ \left.\begin{array}{rcl} \widehat{k}_1 \Delta u_1(x_1) & = & \sigma_{12}(x_1, 0^+) = \sigma_{12}(x_1, 0^-) \\ \widehat{k}_2 \Delta u_2(x_1) & = & \sigma_{22}(x_1, 0^+) = \sigma_{22}(x_1, 0^-) \end{array}\right\} \text{ for } (x_1, 0) \in I_{\text{effective}}, \end{array} \tag{8}$$

where $\Delta u_r(x_1) = u_r(x_1, 0^+) - u_r(x_1, 0^-)$ and

$$\begin{aligned} I_{\text{cracked}} &= \bigcup_{n=-\infty}^{\infty} (c^{(1)} + nL, d^{(1)} + nL), \\ I_{\text{perfect}} &= \bigcup_{n=-\infty}^{\infty} (nL, c^{(1)} + nL) \cup (d^{(1)} + nL, c^{(2)} + nL), \\ I_{\text{effective}} &= \bigcup_{n=-\infty}^{\infty} (c^{(2)} + nL, d^{(2)} + nL). \end{aligned} \tag{9}$$

The plane boundary $x_2 = h$ is acted upon by a suitably prescribed load as given by

$$\sigma_{r2}(x_1, h) = P_r(x_1) \text{ for } -\infty < x_1 < \infty, \tag{10}$$

where $P_r(x_1)$ are periodic functions of x_1 with period L. The component $P_2(x_1)$ is assumed to be positive and providing a sufficiently large external tensile load on the interface (compared to the magnitude of $P_1(x_1)$) so that the assumption $\Delta u_2 > 0$ is valid on I_{cracked} and $I_{\text{effective}}$.

If the displacements u_r and the stresses σ_{rj} are written as

$$\begin{aligned} u_r &= u_r^{(\mathrm{ext})} + u_r^{(\mathrm{imp})}, \\ \sigma_{rj} &= \sigma_{rj}^{(\mathrm{ext})} + \sigma_{rj}^{(\mathrm{imp})}, \end{aligned} \tag{11}$$

where $u_r^{(\mathrm{ext})}$and $\sigma_{rj}^{(\mathrm{ext})}$ are respectively the displacements and stresses satisfying

$$\left.\begin{array}{rcl} \sigma_{r2}^{(\mathrm{ext})}(x_1, h) & = & P_r(x_1) \\ u_r^{(\mathrm{ext})}(x_1, 0^+) & = & u_r^{(\mathrm{ext})}(x_1, 0^-) \\ \sigma_{r2}^{(\mathrm{ext})}(x_1, 0^+) & = & \sigma_{r2}^{(\mathrm{ext})}(x_1, 0^-) \end{array}\right\} \text{ for } -\infty < x_1 < \infty, \tag{12}$$

then (8) and (10) give

$$\begin{array}{l} \sigma_{r2}^{(\mathrm{imp})}(x_1, 0^\pm) = -\sigma_{r2}^{(\mathrm{ext})}(x_1, 0^\pm) \text{ for } (x_1, 0) \in I_{\mathrm{cracked}}, \\ \left.\begin{array}{rcl} \Delta u_r^{(\mathrm{imp})}(x_1) & = & 0 \\ \sigma_{r2}^{(\mathrm{imp})}(x_1, 0^+) & = & \sigma_{r2}^{(\mathrm{imp})}(x_1, 0^-) \end{array}\right\} \text{ for } (x_1, 0) \in I_{\mathrm{perfect}}, \\ \left.\begin{array}{rcl} \widehat{k}_1 \Delta u_1^{(\mathrm{imp})}(x_1) & = & \sigma_{12}^{(\mathrm{ext})}(x_1, 0^\pm) + \sigma_{12}^{(\mathrm{imp})}(x_1, 0^\pm) \\ \widehat{k}_2 \Delta u_2^{(\mathrm{imp})}(x_1) & = & \sigma_{22}^{(\mathrm{ext})}(x_1, 0^\pm) + \sigma_{22}^{(\mathrm{imp})}(x_1, 0^\pm) \end{array}\right\} \text{ for } (x_1, 0) \in I_{\mathrm{effective}}, \end{array} \tag{13}$$

and

$$\sigma_{r2}^{(\mathrm{imp})}(x_1, h) = 0 \text{ for } -\infty < x_1 < \infty, \tag{14}$$

where $\Delta u_r^{(\mathrm{imp})}(x_1) = u_r^{(\mathrm{imp})}(x_1, 0^+) - u_r^{(\mathrm{imp})}(x_1, 0^-)$. Note that $u_r^{(\mathrm{imp})}$and $\sigma_{rj}^{(\mathrm{imp})}$ are respectively the displacements and stresses induced by the micro-cracks and the effective regions.

As the effective stiffness coefficients $\widehat{k}_1$ and $\widehat{k}_2$ are unknown constants to be determined, two more equations are required to complete the formulation of the interfacial conditions for the three-phase model. These equations are

given by

$$\begin{aligned}
\frac{\widehat{k}_1}{c^{(2)}}\int_{c^{(1)}}^{d^{(1)}} \Delta u_1^{(\mathrm{imp})}(x_1)dx_1 &= \frac{1}{c^{(2)}}\int_0^{c^{(2)}} \sigma_{12}^{(\mathrm{ext})}(x_1,0)dx_1,\\
\frac{\widehat{k}_2}{c^{(2)}}\int_{c^{(1)}}^{d^{(1)}} \Delta u_2^{(\mathrm{imp})}(x_1)dx_1 &= \frac{1}{c^{(2)}}\int_0^{c^{(2)}} \sigma_{22}^{(\mathrm{ext})}(x_1,0)dx_1.
\end{aligned} \tag{15}$$

Note that the equations in (15) are derived from

$$\begin{aligned}
&\widehat{k}_p \times (\text{average value of } \Delta u_p^{(\mathrm{imp})}(x_1) \text{ over } 0 < x_1 < c^{(2)})\\
= \;& (\text{average value of } \sigma_{p2}^{(\mathrm{ext})}(x_1,0) \text{ over } 0 < x_1 < c^{(2)}).
\end{aligned} \tag{16}$$

Equation (16) provides a link between the micro-cracked and the effective (macroscopic) parts of the three-phase model. For more details on the role of (16) in the numerical procedure for the three-phase model, refer to Subsection 3.3 below.

For the analysis of the three-phase model, the partial differential equations in (4) together with (2) are to be solved for $u_r^{(\mathrm{imp})}$ in the bimaterial in Figure 2 and for the the unknown effective stiffness coefficients $\widehat{k}_1$ and $\widehat{k}_2$ subject to (13), (14) and (15). Note that the stresses $-\sigma_{r2}^{(\mathrm{ext})}(x_1,0^{\pm})$ may be regarded as prescribed internal loads on the interface and are treated as known functions. For the analysis here, we take $\sigma_{r2}^{(\mathrm{ext})}(x_1,0^{\pm}) = \delta_{r1}S + \delta_{r2}T$, where S and T are positive constants.

3.2 Hypersingular integral and integro-differential equations

To solve the boundary value problem in Section 3.1, the boundary integral equations in Clements [6] are used together with the perfect interface Green's

function in Berger and Tewary [2] to derive the integral solution

$$
\begin{aligned}
u_j^{(\mathrm{imp})}(\xi_1,\xi_2) &= \frac{1}{2\pi}\sum_{n=-\infty}^{\infty}\int_{nL}^{(n+1)L} u_r^{(\mathrm{imp})}(x_1,h) \\
&\quad \times \mathrm{Re}\{\sum_{\alpha=1}^{2} L_{r2\alpha}^{(1)}[\frac{N_{\alpha p}^{(1)}}{x_1-\xi_1+\tau_\alpha^{(1)}(h-\xi_2)} \\
&\quad + \sum_{\beta=1}^{2} Q_{\alpha\beta p}^{(1)} \frac{1}{x_1-\xi_1+\tau_\alpha^{(1)}h-\overline{\tau}_\beta^{(1)}\xi_2}]\}D_{pj}^{(1)}dx_1 \\
&\quad -\frac{1}{2\pi}\sum_{n=-\infty}^{\infty}\sum_{k=1}^{2}\int_{c^{(k)}+nL}^{d^{(k)}+nL} \Delta u_r^{(\mathrm{imp})}(x_1) \\
&\quad \times \mathrm{Re}\{\sum_{\alpha=1}^{2} L_{r2\alpha}^{(1)}[\frac{N_{\alpha p}^{(1)}}{x_1-\xi_1-\tau_\alpha^{(1)}\xi_2} \\
&\quad + \sum_{\beta=1}^{2} Q_{\alpha\beta p}^{(1)} \frac{1}{x_1-\xi_1-\overline{\tau}_\beta^{(1)}\xi_2}]\}D_{pj}^{(1)}dx_1 \\
&\quad \text{for } 0<\xi_2<h, \qquad (17)
\end{aligned}
$$

where Re denotes the real part of a complex number, the overhead bar denotes the complex conjugate of a complex number, the constants $Q_{\alpha\beta p}^{(1)}$ are implicitly defined by (see Chen and Ang [3])

$$
\sum_{\alpha=1}^{2}(\overline{A}_{k\alpha}^{(1)}N_{\gamma k}^{(2)}-\overline{L}_{k2\alpha}^{(1)}M_{\gamma k}^{(2)})\overline{Q}_{\alpha\beta p}^{(1)} = (L_{k2\beta}^{(1)}M_{\gamma k}^{(2)}-A_{k\beta}^{(1)}N_{\gamma k}^{(2)})N_{\beta p}^{(1)}, \qquad (18)
$$

the constants $A_{m\alpha}^{(q)}$ are chosen to be given by

$$
[A_{m\alpha}^{(q)}] = \begin{bmatrix} -\dfrac{i\tau_1^{(q)}[C_{12}^{(q)}+C_{66}^{(q)}]}{C_{11}^{(q)}+C_{66}^{(q)}(\tau_1^{(q)})^2} & -\dfrac{i\tau_2^{(q)}[C_{12}^{(q)}+C_{66}^{(q)}]}{C_{11}^{(q)}+C_{66}^{(q)}(\tau_2^{(q)})^2} \\ i & i \end{bmatrix}, \qquad (19)
$$

$i=\sqrt{-1}$, $L_{i2\alpha}^{(q)}$ are given by

$$
\begin{aligned}
L_{12\alpha}^{(q)} &= C_{66}^{(q)}(\tau_\alpha^{(q)}A_{1\alpha}^{(q)}+A_{2\alpha}^{(q)}), \\
L_{22\alpha}^{(q)} &= C_{12}^{(q)}A_{1\alpha}^{(q)}+\tau_\alpha^{(q)}C_{22}^{(q)}A_{2\alpha}^{(q)}, \qquad (20)
\end{aligned}
$$

the constants $\tau_1^{(q)}$ and $\tau_2^{(q)}$ are two distinct complex numbers with positive imaginary parts and are solutions of the quartic equation in τ given by

$$C_{22}^{(q)}C_{66}^{(q)}\tau^4 - ([C_{12}^{(q)}]^2 + 2C_{12}^{(q)}C_{66}^{(q)} - C_{22}^{(q)}C_{11}^{(q)})\tau^2 + C_{11}^{(q)}C_{66}^{(q)} = 0, \qquad (21)$$

the matrices $[N_{\alpha p}^{(q)}]$ and $[M_{\alpha p}^{(q)}]$ are the inverses of $[A_{k\alpha}^{(q)}]$ and $[L_{k2\alpha}^{(q)}]$ respectively, and the constants $D_{rp}^{(q)}$ are defined implicitly by

$$\mathrm{Im}\{\sum_{\alpha=1}^{2} L_{i2\alpha}^{(q)} N_{\alpha r}^{(q)}\} D_{rp}^{(q)} = \delta_{ip}, \qquad (22)$$

where δ_{ip} is Kronecker-delta and Im denotes the imaginary part of a complex number.

Note that lowercase Greek and Latin subscripts have values 1 and 2 and the Einsteinian convention of summing over a repeated index is applicable here only for lowercase Latin subscripts.

According to the generalised Hooke's law, (17) gives rise to the stress formula

$$\begin{aligned}
\sigma_{i2}^{(\mathrm{imp})}(\xi_1,\xi_2) \;=\; & \frac{1}{2\pi}\,\mathrm{Re}\{\sum_{n=-\infty}^{\infty}\int_{nL}^{(n+1)L} u_r^{(\mathrm{imp})}(x_1,h) \\
& \times[\sum_{\alpha=1}^{2}\frac{G_{ri\alpha}}{(x_1-\xi_1+\tau_\alpha^{(1)}(h-\xi_2))^2} \\
& +\sum_{\alpha=1}^{2}\sum_{\beta=1}^{2}\frac{H_{ri\alpha\beta}}{(x_1-\xi_1+\tau_\alpha^{(1)}h-\overline{\tau}_\beta^{(1)}\xi_2)^2}]dx_1\} \\
& -\frac{1}{2\pi}\,\mathrm{Re}\{\sum_{n=-\infty}^{\infty}\sum_{k=1}^{2}\int_{c^{(k)}+nL}^{d^{(k)}+nL}\Delta u_r^{(\mathrm{imp})}(x_1) \\
& \times[\sum_{\alpha=1}^{2}\frac{G_{ri\alpha}}{(x_1-\xi_1-\tau_\alpha^{(1)}\xi_2)^2} \\
& +\sum_{\alpha=1}^{2}\sum_{\beta=1}^{2}\frac{H_{ri\alpha\beta}}{(x_1-\xi_1-\overline{\tau}_\beta^{(1)}\xi_2)^2}]dx_1\} \\
& \qquad \text{for } 0<\xi_2<h, \qquad (23)
\end{aligned}$$

where

$$\begin{aligned} G_{r1\alpha} &= L^{(1)}_{r2\alpha} N^{(1)}_{\alpha p} C^{(1)}_{66} (\tau^{(1)}_{\alpha} D^{(1)}_{p1} + D^{(1)}_{p2}), \\ G_{r2\alpha} &= L^{(1)}_{r2\alpha} N^{(1)}_{\alpha p} (C^{(1)}_{12} D^{(1)}_{p1} + \tau^{(1)}_{\alpha} C^{(1)}_{22} D^{(1)}_{p2}), \\ H_{r1\alpha\beta} &= L^{(1)}_{r2\alpha} Q^{(1)}_{\alpha\beta p} C^{(1)}_{66} (\overline{\tau}^{(1)}_{\beta} D^{(1)}_{p1} + D^{(1)}_{p2}), \\ H_{r2\alpha\beta} &= L^{(1)}_{r2\alpha} Q^{(1)}_{\alpha\beta p} (C^{(1)}_{12} D^{(1)}_{p1} + \overline{\tau}^{(1)}_{\beta} C^{(1)}_{22} D^{(1)}_{p2}). \end{aligned} \tag{24}$$

From (23) and the summation formula (Wang *et al* [21])

$$\sum_{n=1}^{\infty} \frac{1}{(a \pm bn)^2} = \frac{1}{b^2} \Psi_1(1 \pm \frac{a}{b}) \text{ for } \mathrm{Re}\{1 \pm \frac{a}{b}\} > 0, \tag{25}$$

where Ψ_1 is the trigamma function, the conditions in (13) and (14) may be expressed in terms of the hypersingular integral equations

$$\begin{aligned} & \frac{1}{2\pi} \Xint-_0^{d^{(2)}} u_r^{(\mathrm{imp})}(x_1, h) \, \mathrm{Re}\{\sum_{\alpha=1}^{2} G_{ri\alpha}\} [\frac{1}{(x_1 - \xi_1)^2} + \Theta(x_1, \xi_1)] dx_1 \\ & + \frac{1}{2\pi} \int_0^{d^{(2)}} u_r^{(\mathrm{imp})}(x_1, h) \, \mathrm{Re}\{\sum_{\alpha=1}^{2} \sum_{\beta=1}^{2} H_{ri\alpha\beta} \Omega(x_1, \xi_1, \tau^{(1)}_{\alpha} h - \overline{\tau}^{(1)}_{\beta} h)\} dx_1 \\ & - \frac{1}{2\pi} \sum_{k=1}^{2} \int_{c^{(k)}}^{d^{(k)}} \Delta u_r^{(\mathrm{imp})}(x_1) \, \mathrm{Re}\{\sum_{\alpha=1}^{2} G_{ri\alpha} \Omega(x_1, \xi_1, -\tau^{(1)}_{\alpha} h)\} dx_1 \\ & - \frac{1}{2\pi} \sum_{k=1}^{2} \int_{c^{(k)}}^{d^{(k)}} \Delta u_r^{(\mathrm{imp})}(x_1) \, \mathrm{Re}\{\sum_{\alpha=1}^{2} \sum_{\beta=1}^{2} H_{ri\alpha\beta} \Omega(x_1, \xi_1, -\overline{\tau}^{(1)}_{\beta} h)\} dx_1 \\ = \; & 0 \quad \text{for } 0 < \xi_1 < d^{(2)}, \end{aligned} \tag{26}$$

and the hypersingular integro-differential equations

$$
\begin{aligned}
&-\frac{1}{2\pi}\int_0^{d^{(2)}} u_r^{(\mathrm{imp})}(x_1,h)\,\mathrm{Re}\{\sum_{\alpha=1}^{2}\Omega(x_1,\xi_1,\tau_\alpha^{(1)}h)(G_{ri\alpha}+\sum_{\beta=1}^{2}H_{ri\alpha\beta})\}dx_1\\
&+\frac{1}{2\pi}[\Xint=_{c^{(k)}}^{d^{(k)}}\frac{\Delta u_r^{(\mathrm{imp})}(x_1)\,\mathrm{Re}\{W_{ri}\}}{(x_1-\xi_1)^2}dx_1\\
&+\sum_{\substack{n=1\\n\neq k}}^{2}\int_{c^{(n)}}^{d^{(n)}}\frac{\Delta u_r^{(\mathrm{imp})}(x_1)\,\mathrm{Re}\{W_{ri}\}}{(x_1-\xi_1)^2}dx_1\\
&+\sum_{n=1}^{2}\int_{c^{(n)}}^{d^{(n)}}\Delta u_r^{(\mathrm{imp})}(x_1)\,\mathrm{Re}\{W_{ri}\}\Theta(x_1,\xi_1)dx_1-\frac{d\Delta u_r^{(\mathrm{imp})}(\xi_1)}{d\xi_1}\,\mathrm{Im}\{\pi V_{ri}\}]\\
=\;&\delta_{i1}S+\delta_{i2}T-\delta^{(k2)}k_{ij}\Delta u_j^{(\mathrm{imp})}(\xi_1) \qquad (27)\\
&\text{for } c^{(k)}<\xi_1<d^{(k)}\ (k=1,2)
\end{aligned}
$$

where $\Xint=$ denotes that the integral is to be interpreted in the Hadamard finite-part sense, $k_{11}=\widehat{k}_1$, $k_{12}=k_{21}=0$ and $k_{22}=\widehat{k}_2$, $\delta^{(k2)}$ is such that $\delta^{(12)}=0$ and $\delta^{(22)}=1$, $\Theta(x_1,\xi_1)$ and $\Omega(x_1,\xi_1,z)$ are defined by

$$
\begin{aligned}
\Theta(x_1,\xi_1) &= \frac{1}{L^2}\Psi_1(\frac{L+x_1-\xi_1}{L})+\frac{1}{L^2}\Psi_1(\frac{L+\xi_1-x_1}{L}),\\
\Omega(x_1,\xi_1,z) &= \frac{1}{(x_1-\xi_1+z)^2}+\frac{1}{L^2}\Psi_1(\frac{L+x_1-\xi_1+z}{L})\\
&\quad+\frac{1}{L^2}\Psi_1(\frac{L-x_1+\xi_1-z}{L}), \qquad (28)
\end{aligned}
$$

and the constants W_{ri} and V_{ri} are given by

$$
\begin{aligned}
W_{ri} &= \sum_{\alpha=1}^{2}G_{ri\alpha}+\sum_{\alpha=1}^{2}\sum_{\beta=1}^{2}H_{ri\alpha\beta},\\
V_{ri} &= \sum_{\alpha=1}^{2}\sum_{\beta=1}^{2}H_{ri\alpha\beta}-\sum_{\alpha=1}^{2}G_{ri\alpha}. \qquad (29)
\end{aligned}
$$

3.3 Numerical procedure

A numerical procedure for solving the hypersingular integral and integro-differential equations in (26) and (27) together with (15) is outlined here.

The part of the edge of the thin layer, where $0 \le x_1 \le d^{(2)}$, $x_2 = h$, is discretized into $N_{\rm t}$ subintervals (elements) given by

$$x_{\rm t}^{(p)} \le x_1 \le x_{\rm t}^{(p+1)},\ x_2 = h \quad (p = 1, 2, \cdots, N_{\rm t}). \tag{30}$$

The unknown functions $u_r^{(\rm imp)}(x_1, h)$ for $0 \le x_1 \le d^{(2)}$ are approximated as linear functions of x_1 over the p-th element, that is,

$$u_r^{(\rm imp)}(x_1, h) \simeq x_1 \phi_r^{(p)} + \psi_r^{(p)} \text{ for } x_{\rm t}^{(p)} \le x_1 \le x_{\rm t}^{(p+1)}, \tag{31}$$

where $\phi_r^{(p)}$ and $\psi_r^{(p)}$ are $4N_{\rm t}$ unknown constants to be determined. Two collocation points are chosen on the p-th element, namely

$$\left.\begin{aligned} (\widetilde{x}_{\rm t}^{(p)}, h) &= (\frac{3}{4}x_{\rm t}^{(p)} + \frac{1}{4}x_{\rm t}^{(p+1)}, h) \\ (\widetilde{x}_{\rm t}^{(p+N_{\rm t})}, h) &= (\frac{1}{4}x_{\rm t}^{(p)} + \frac{3}{4}x_{\rm t}^{(p+1)}, h) \end{aligned}\right\} \text{for } p = 1, 2, ..., N_{\rm t}, \tag{32}$$

in order to collocate (26) at $2N_{\rm t}$ points in the interval $0 < \xi_1 < d^{(2)}$.

The crack opening displacements $\Delta u_r^{(\rm imp)}(x_1)$ for $c^{(1)} < x_1 < d^{(1)}$ (over the representative micro-crack in the three-phase model) are approximated as in Kaya and Erdogan [14] by

$$\begin{aligned} \Delta u_r^{(\rm imp)}(x_1) \ &\simeq \ \sqrt{(x_1 - c^{(1)})(d^{(1)} - x_1)} \sum_{m=1}^{N_{\rm c}} \alpha_r^{(m)} U^{(m-1)}(\frac{2x_1 - d^{(1)} - c^{(1)}}{d^{(1)} - c^{(1)}}) \\ &\text{for } c^{(1)} < x_1 < d^{(1)}, \end{aligned} \tag{33}$$

where $\alpha_r^{(m)}$are $2N_{\rm c}$ unknown constants to be determined and $U^{(m)}(x_1)$ is the m-th order Chebyshev polynomial of the second kind. For collocating (27) at

N_c points on the representative micro-crack, the following collocation points are defined:

$$(\widetilde{x}_{\rm c}^{(km)}, 0) \;=\; (\frac{d^{(1)}+c^{(1)}}{2} + \frac{d^{(1)}-c^{(1)}}{2}\cos(\frac{[2m-1]\pi}{2N_{\rm c}}), 0) \quad \text{for } m = 1, 2, \cdots, N_{\rm c}. \tag{34}$$

Details on the numerical treatment involved in approximation in (33) may also be found in Ang [1].

The effective region $c^{(2)} < x_1 < d^{(2)}$, $x_2 = 0$, is discretized into $N_{\rm e}$ subintervals (elements) given by

$$x_{\rm e}^{(p)} \le x_1 \le x_{\rm e}^{(p+1)},\ x_2 = h \ \ (p = 1, 2, \cdots, N_{\rm e}), \tag{35}$$

where

$$x_{\rm e}^{(p)} \;=\; \frac{d^{(2)}+c^{(2)}}{2} - \frac{d^{(2)}-c^{(2)}}{2}\cos(\frac{[p-1]\pi}{N_{\rm e}}) \quad \text{for } p = 1, 2, ..., N_{\rm e}+1. \tag{36}$$

The displacement jumps $\Delta u_r^{(\rm imp)}(x_1)$ over the p-th element on the effective region are approximated by

$$\Delta u_r^{(\rm imp)}(x_1) \simeq x_1 \vartheta_r^{(p)} + \eta_r^{(p)} \text{ for } x_{\rm e}^{(p)} \le x_1 \le x_{\rm e}^{(p+1)}, \tag{37}$$

where $\vartheta_r^{(p)}$ and $\eta_r^{(p)}$ are $4N_{\rm e}$ unknown constants yet to be determined. To ensure that $\Delta u_r^{(\rm imp)}(x_1) = 0$ at the endpoints $x_1 = x_{\rm e}^{(1)}$ and $x_1 = x_{\rm e}^{(Ne+1)}$,we require that

$$x_{\rm e}^{(1)}\vartheta_r^{(1)} + \eta_r^{(1)} = 0 \text{ and } x_{\rm e}^{(Ne+1)}\vartheta_r^{(Ne+1)} + \eta_r^{(Ne+1)} = 0. \tag{38}$$

In view of (38), the hypersingular integro-differential equations in (27) have to be collocated at only $2N_{\rm e} - 2$ points on the effective region. The $2N_{\rm e} - 2$

collocation points on the effective region are given by

$$\begin{aligned}(\widetilde{x}_{\rm e}^{(1)},0) &= (\frac{1}{2}x_{\rm e}^{(1)}+\frac{1}{2}x_{\rm e}^{(2)},0),\\ (\widetilde{x}_{\rm e}^{(2N_{\rm e}-2)},0) &= (\frac{1}{2}x_{\rm e}^{(N_{\rm e})}+\frac{1}{2}x_{\rm e}^{(N_{\rm e}+1)},0),\end{aligned} \tag{39}$$

and

$$\left.\begin{aligned}(\widetilde{x}_{\rm e}^{(p+1)},0) &= (\frac{3}{4}x_{\rm e}^{(p+1)}+\frac{1}{4}x_{\rm e}^{(p+2)},0)\\ (\widetilde{x}_{\rm e}^{(p+N_{\rm e}-1)},0) &= (\frac{1}{4}x_{\rm e}^{(p+1)}+\frac{3}{4}x_{\rm e}^{(p+2)},0)\end{aligned}\right\} \text{for } p=1,...,N_{\rm e}-2. \tag{40}$$

If the effective stiffness coefficients $\widehat{k}_j$ are assumed known, we may substitute (31), (33), (37) and (38) into (26) and (27) and collocate the resulting equations appropriately at the selected collocation points to obtain a system of linear algebraic equations. The linear algebraic equations are solved for the unknown constants in (31), (33), (37) and (38). Once the unknown constants are determined, the values of $\widehat{k}_j$ are updated using (15). The linear algebraic equations are then solved again using the updated values of $\widehat{k}_j$. The iteration between solving the linear algebraic equations and updating the values of $\widehat{k}_j$ is repeated until the values of $\widehat{k}_j$ converge to within a prescribed number of significant figures.

4 Micromechanical-statistical model

4.1 Statistical simulation of the interface

In the micromechanical-statistical model, the M micro-cracks in the region $0 < x_1 < L$, $x_2 = 0$, in Figure 1 are generated randomly. Specifically, the lengths of M micro-cracks are randomly generated to follow a chi-square distribution of degree of freedom k, which is denoted here by $\chi^2(k)$, and are randomly positioned in the region $0 < x_1 < L$, $x_2 = 0$. As explained in Wang *et al* [22], the χ^2 distribution with a lower degree of freedom has a more skewed probability density function, giving a greater number of shorter micro-cracks. The randomly selected and positioned micro-cracks form a randomly generated interface.

For fixed values of the material constants in the layer and the elastic half-space, the average length of the micro-cracks, the thickness of the layer, the period length L of the interface and the number of micro-cracks on a period length of the interface, N interfaces are randomly generated to form a statistical sample for examining the effective stiffness coefficients of the interface. The effective stiffness coefficients $\widehat{k}_1$ and $\widehat{k}_2$ of the n-th interface may be computed by solving a system of hypersingular integral and integro-differential equations as explained in Subsection 4.2 and 4.3 below. If the appropriately non-dimensionalized values of the effective stiffness coefficients $\widehat{k}_j$ of the N interfaces are given by $Y_j^{(1)}$, $Y_j^{(2)}$, ..., $Y_j^{(N-1)}$ and $Y_j^{(N)}$, then the mean value μ_j and standard deviation s_j of the non-dimensionalized effective stiffness coefficients are respectively given by

$$\mu_j = \frac{1}{N}\sum_{n=1}^{N} Y_j^{(n)} \text{ and } s_j = \sqrt{\frac{1}{N-1}\sum_{n=1}^{N}(Y_j^{(n)} - \mu_j)^2}. \tag{41}$$

4.2 Boundary value problem

As in the three-phase model, the displacements u_r and the stresses σ_{rj} are written in the form (11), where $u_r^{(\mathrm{ext})}$and $\sigma_{rj}^{(\mathrm{ext})}$ are required to satisfy (12) and $u_r^{(\mathrm{imp})}$and $\sigma_{rj}^{(\mathrm{imp})}$ are respectively the displacements and stresses induced by the interface micro-cracks. As in Section 3.1, the stresses $\sigma_{rj}^{(\mathrm{ext})}$ are such that $\sigma_{r2}^{(\mathrm{ext})}(x_1, 0^{\pm}) = \delta_{r1}S + \delta_{r2}T$, where S and T are positive constants.

The interfacial conditions on $u_r^{(\mathrm{imp})}$and $\sigma_{rj}^{(\mathrm{imp})}$ are given by

$$\begin{aligned} \sigma_{r2}^{(\mathrm{imp})}(x_1, 0^{\pm}) &= -\delta_{r1}S - \delta_{r2}T \text{ for } a^{(k)} + nL < x_1 < b^{(k)} + nL \\ &\quad (k = 1, 2, \cdots, M;\ n = 0, \pm 1, \pm 2, \cdots .), \end{aligned} \tag{42}$$

and

$$\begin{aligned} \Delta u_r^{(\mathrm{imp})}(x_1) = 0 \text{ and } \sigma_{r2}^{(\mathrm{imp})}(x_1, 0^+) = \sigma_{r2}^{(\mathrm{imp})}(x_1, 0^-) \\ \text{on the uncracked parts of the interface.} \end{aligned} \tag{43}$$

The partial differential equations (4) together with (2) are solved in the bimaterial subject to the conditions in (14), (42) and (43). Once the displacement jumps $\Delta u_r^{(\mathrm{imp})}(x_1)$ are known on the M micro-cracks, the effective stiffness coefficients may be evaluated by using

$$\begin{aligned} \frac{\widehat{k}_1}{L} \sum_{k=1}^{M} \int_{a^{(k)}}^{b^{(k)}} \Delta u_1^{(\mathrm{imp})}(x_1) dx_1 &= S, \\ \frac{\widehat{k}_2}{L} \sum_{k=1}^{M} \int_{a^{(k)}}^{b^{(k)}} \Delta u_2^{(\mathrm{imp})}(x_1) dx_1 &= T. \end{aligned} \tag{44}$$

For the micromechanical-statistical model, the damage ratio ρ of the interface, which corresponds to (7) for the three-phase model, is given by

$$\rho = \frac{1}{L} \sum_{k=1}^{M} (b^{(k)} - a^{(k)}). \tag{45}$$

4.3 Hypersingular integral and integro-differential equations

As in the analysis for the three-phase model, the use of the boundary integral equations and the perfect interface Green's function in Berger and Tewary [2] with the micro-cracked interface in Figure 1 gives

$$
\begin{aligned}
u_j^{(\mathrm{imp})}(\xi_1,\xi_2) \;=\; & \frac{1}{2\pi}\sum_{n=-\infty}^{\infty}\int_{nL}^{(n+1)L} u_r^{(\mathrm{imp})}(x_1,h) \\
& \times \mathrm{Re}\{\sum_{\alpha=1}^{2} L_{r2\alpha}^{(1)}[\frac{N_{\alpha p}^{(1)}}{x_1-\xi_1+\tau_\alpha^{(1)}(h-\xi_2)} \\
& + \sum_{\beta=1}^{2} Q_{\alpha\beta p}^{(1)} \frac{1}{x_1-\xi_1+\tau_\alpha^{(1)}h-\overline{\tau}_\beta^{(1)}\xi_2}]\}D_{pj}^{(1)}dx_1 \\
& - \frac{1}{2\pi}\sum_{n=-\infty}^{\infty}\sum_{k=1}^{M}\int_{a^{(k)}+nL}^{b^{(k)}+nL} \Delta u_r^{(\mathrm{imp})}(x_1) \\
& \times \mathrm{Re}\{\sum_{\alpha=1}^{2} L_{r2\alpha}^{(1)}[\frac{N_{\alpha p}^{(1)}}{x_1-\xi_1-\tau_\alpha^{(1)}\xi_2} \\
& + \sum_{\beta=1}^{2} Q_{\alpha\beta p}^{(1)} \frac{1}{x_1-\xi_1-\overline{\tau}_\beta^{(1)}\xi_2}]\}D_{pj}^{(1)}dx_1 \\
& \text{for } 0<\xi_2<h, \qquad (46)
\end{aligned}
$$

and

$$\begin{aligned}
\sigma_{i2}^{(\mathrm{imp})}(\xi_1,\xi_2) &= \frac{1}{2\pi}\,\mathrm{Re}\{\sum_{n=-\infty}^{\infty}\int_{nL}^{(n+1)L} u_r^{(\mathrm{imp})}(x_1,h)\\
&\quad\times[\sum_{\alpha=1}^{2}\frac{G_{ri\alpha}}{(x_1-\xi_1+\tau_\alpha^{(1)}(h-\xi_2))^2}\\
&\quad+\sum_{\alpha=1}^{2}\sum_{\beta=1}^{2}\frac{H_{ri\alpha\beta}}{(x_1-\xi_1+\tau_\alpha^{(1)}h-\overline{\tau}_\beta^{(1)}\xi_2)^2}]dx_1\}\\
&\quad-\frac{1}{2\pi}\,\mathrm{Re}\{\sum_{n=-\infty}^{\infty}\sum_{k=1}^{M}\int_{a^{(k)}+nL}^{b^{(k)}+nL}\Delta u_r^{(\mathrm{imp})}(x_1)\\
&\quad\times[\sum_{\alpha=1}^{2}\frac{G_{ri\alpha}}{(x_1-\xi_1-\tau_\alpha^{(1)}\xi_2)^2}\\
&\quad+\sum_{\alpha=1}^{2}\sum_{\beta=1}^{2}\frac{H_{ri\alpha\beta}}{(x_1-\xi_1-\overline{\tau}_\beta^{(1)}\xi_2)^2}]dx_1\}\\
&\quad\text{for } 0<\xi_2<h. \qquad (47)
\end{aligned}$$

From (25) and (47), the conditions (14) and (42) on a given interface may be expressed in terms of the hypersingular integral equations

$$\begin{aligned}
&\frac{1}{2\pi}\Xint=_0^L u_r^{(\mathrm{imp})}(x_1,h)\,\mathrm{Re}\{\sum_{\alpha=1}^{2}G_{ri\alpha}\}[\frac{1}{(x_1-\xi_1)^2}+\Theta(x_1,\xi_1)]dx_1\\
&+\frac{1}{2\pi}\int_0^L u_r^{(\mathrm{imp})}(x_1,h)\,\mathrm{Re}\{\sum_{\alpha=1}^{2}\sum_{\beta=1}^{2}H_{ri\alpha\beta}\Omega(x_1,\xi_1,\tau_\alpha^{(1)}h-\overline{\tau}_\beta^{(1)}h)\}dx_1\\
&-\frac{1}{2\pi}\sum_{k=1}^{M}\int_{a^{(k)}}^{b^{(k)}}\Delta u_r^{(\mathrm{imp})}(x_1)\,\mathrm{Re}\{\sum_{\alpha=1}^{2}G_{ri\alpha}\Omega(x_1,\xi_1,-\tau_\alpha^{(1)}h)\}dx_1\\
&-\frac{1}{2\pi}\sum_{k=1}^{M}\int_{a^{(k)}}^{b^{(k)}}\Delta u_r^{(\mathrm{imp})}(x_1)\,\mathrm{Re}\{\sum_{\alpha=1}^{2}\sum_{\beta=1}^{2}H_{ri\alpha\beta}\Omega(x_1,\xi_1,-\overline{\tau}_\beta^{(1)}h)\}dx_1\\
=\;&0\quad\text{for } 0<\xi_1<L, \qquad (48)
\end{aligned}$$

and the hypersingular integro-differential equations

$$
\begin{aligned}
&-\frac{1}{2\pi}\int_0^L u_r^{(\mathrm{imp})}(x_1,h)\,\mathrm{Re}\{\sum_{\alpha=1}^{2}\Omega(x_1,\xi_1,\tau_\alpha^{(1)}h)(G_{ri\alpha}+\sum_{\beta=1}^{2}H_{ri\alpha\beta})\}dx_1 \\
&+\frac{1}{2\pi}[\neq\!\!\int_{a^{(k)}}^{b^{(k)}}\frac{\Delta u_r^{(\mathrm{imp})}(x_1)\,\mathrm{Re}\{W_{ri}\}}{(x_1-\xi_1)^2}dx_1 \\
&+\sum_{\substack{n=1\\n\neq k}}^{M}\int_{a^{(n)}}^{b^{(n)}}\frac{\Delta u_r^{(\mathrm{imp})}(x_1)\,\mathrm{Re}\{W_{ri}\}}{(x_1-\xi_1)^2}dx_1 \\
&+\sum_{n=1}^{M}\int_{a^{(n)}}^{b^{(n)}}\Delta u_r^{(\mathrm{imp})}(x_1)\,\mathrm{Re}\{W_{ri}\}\Theta(x_1,\xi_1)dx_1-\frac{d\Delta u_r^{(\mathrm{imp})}(\xi_1)}{d\xi_1}\,\mathrm{Im}\{\pi V_{ri}\}] \\
=\;&\delta_{i1}S+\delta_{i2}T \text{ for } a^{(k)}<\xi_1<b^{(k)}\ (k=1,2,...,M) \qquad (49)
\end{aligned}
$$

Once the unknown functions $\Delta u_r^{(\mathrm{imp})}(x_1)$ over the micro-cracks are obtained by solving (48) and (49), the effective stiffness coefficients $\widehat{k}_1$ and $\widehat{k}_2$ of the given interface may be calculated by using (44).

4.4 Numerical procedure

For the micromechanical-statistical model, the hypersingular integral and integro-differential equations (48) and (49) for a given interface may be solved by using the numerical procedure outlined below.

As in Subsection 3.3, the region $0 \le x_1 \le L$, $x_2 = h$ on the edge of the layer is discretized into N_{t} elements as given in (30), the unknown functions $u_r^{(\mathrm{imp})}(x_1,h)$ for $0 \le x_1 \le L$ are approximated as linear functions of x_1 as given in (31), and the $2N_{\mathrm{t}}$ collocation points for collocating the hypersingular integral equations (48) are given by (32).

The crack opening displacements $\Delta u_r^{(\mathrm{imp})}(x_1)$ over the M micro-cracks

are approximated using

$$\begin{aligned}\Delta u_r^{(\mathrm{imp})}(x_1) &\simeq \sqrt{(x_1-a^{(k)})(b^{(k)}-x_1)} \\ &\quad \times \sum_{m=1}^{N_c^{(k)}} \alpha_r^{(km)} U^{(m-1)}\Big(\frac{2x_1-b^{(k)}-a^{(k)}}{b^{(k)}-a^{(k)}}\Big) \\ \text{for } a^{(k)} &< x_1 < b^{(k)} \ (k=1,2,...,M), \end{aligned} \tag{50}$$

where $\alpha_r^{(km)}$ $(r=1,2;\ m=1,2,...,N_{\mathrm{c}}^{(k)};\ k=1,2,...,M)$ are unknowns to be determined and $N_{\mathrm{c}}^{(k)}$ are positive integers. For a fixed k, the hypersingular integro-differential equations in (49) are collocated at $N_{\mathrm{c}}^{(k)}$ selected points on the k-th micro-crack. The $N_{\mathrm{c}}^{(k)}$ collocation points are given by

$$\begin{aligned}(\widetilde{x}_{\mathrm{c}}^{(km)}, 0) &= \Big(\frac{a^{(k)}+b^{(k)}}{2} + \frac{b^{(k)}-a^{(k)}}{2}\cos\Big(\frac{[2m-1]\pi}{2N_{\mathrm{c}}^{(k)}}\Big), 0\Big) \\ &\qquad \text{for } m=1,2,\cdots,N_{\mathrm{c}}^{(k)} \ (k=1,2,...,M). \end{aligned} \tag{51}$$

If we substitute the approximations (31) and (50) into (48) and (49) and collocate the resulting equations at the selected collocation points, the hypersingular integral and integro-differential equations (48) and (49) may be eventually reduced into a system of linear algebraic equations containing $4N_{\mathrm{t}}+2N_{\mathrm{c}}^{(1)}+2N_{\mathrm{c}}^{(2)}+...+2N_{\mathrm{c}}^{(M)}$ unknowns. Once the crack opening displacements $\Delta u_r^{(\mathrm{imp})}(x_1)$ are obtained by solving the linear algebraic equations, the effective stiffness coefficients $\widehat{k}_1$ and $\widehat{k}_2$ of the given interface may then be calculated approximately by using (44).

5 A numerical verification of the models

The effective stiffness coefficients $\widehat{k}_1$ and $\widehat{k}_2$ obtained using the micromechanical model in Section 4 are expected to be close to the ones predicted using the three-phase model (in Section 3), if all the micro-cracks in the micromechanical model are taken to be of equal length and are evenly distributed

along the damaged interface. To check this for a particular combination of materials, the elastic moduli (in GPa) for graphite-epoxy and E-glass-epoxy, as given in Table 1 in Section 5 below, are used as the material constants for the orthotropic thin layer and half-space respectively. The values of the elastic moduli for the materials given in Table 1 are taken from Glodež *et al.* [9], Guechaichia and Trendafilova [10] and Rubio-Gonzalez and Mason [17].

For the three-phase model, the length of the representative micro-crack is given by $2a$. The constants $c^{(1)}$, $d^{(1)}$, $c^{(2)}$ and $d^{(1)}$ in Figure 2 are taken as $c^{(1)} = b - a$, $d^{(1)} = b + a$, $c^{(2)} = 2b$ and $d^{(2)} = L$, where b is a positive number much smaller than the period length L. The damage ratio ρ is given here by a/b. For selected a/h (h is the thickness of the thin layer) and ρ, the non-dimensionalized effective stiffness coefficients $a\widehat{k}_1/C_{66}^{(2)}$ and $a\widehat{k}_2/C_{66}^{(2)}$ are computed as outlined in Subsection 3.3.

For the micromechanical model in Section 4, 10 micro-cracks, each of length $2a$, are evenly distributed over the region $0 < x_1 < L$ of the interface. For selected a/h and ρ, the non-dimensionalized effective stiffness coefficients $a\widehat{k}_1/C_{66}^{(2)}$ and $a\widehat{k}_2/C_{66}^{(2)}$ are computed using (44), once the hypersingular integral and integro-differential equations for the micromechanical model are solved numerically as outlined in Subsection 4.4.

Figure 3 gives the plots of the non-dimensionalized effective stiffness coefficients $a\widehat{k}_1/C_{66}^{(2)}$ and $a\widehat{k}_2/C_{66}^{(2)}$ against a/h for damage ratio $\rho = 0.3$, 0.5 and 0.7. As expected, the non-dimensionalized effective stiffness coefficients calculated using the micromechanical model in Section 4 agree well with the corresponding values predicted by the three-phase model. The percentage difference of the non-dimensionalized effective stiffness coefficients between the two models is found to range from 0.012% to 5.5% for $0 < a/h \leq 5$ and $0.1 \leq \rho \leq 0.9$, with the percentage difference becoming larger as the damage

ratio ρ increases.

From Figure 3, for a fixed value of a/h, each of the non-dimensionalized effective stiffness coefficients $a\widehat{k}_1/C_{66}^{(2)}$ and $a\widehat{k}_2/C_{66}^{(2)}$ is observed to decrease in magnitude as the damage ratio ρ increases. This is because the coplanar interfacial micro-cracks for larger value of ρ are closer to one another and interact more strongly with one another in such a way that the magnitudes of the displacement jumps increase. It is also observed that $a\widehat{k}_1/C_{66}^{(2)}$ and $a\widehat{k}_2/C_{66}^{(2)}$ decrease as a/h increases. For a larger value of a/h, the edge of the thin layer is closer to the micro-cracks, giving rise to larger displacement jumps across the micro-damaged parts of the interface. Note that $a/h \to 0^+$ corresponds to the case where the bimaterial is made up of two elastic half-spaces.

6 Micromechanical-statistical simulations

The micromechanical-statistical approach in Section 4 is used in this section for estimating the effective stiffness coefficients of the micro-cracked interface. As explained in Subsection 4.1, an interface is formed by choosing the M micro-cracks over a period interval of the interface to have randomly generated sizes. More specifically, the length of a micro-crack follows a χ^2 distribution of a fixed degree of freedom. The M micro-cracks are then randomly positioned over a period length L of the interface. The average half-length $\widehat{a}$ of the M micro-cracks are related to the period length L and the damage ratio ρ of the interface by

$$\rho L = 2M\widehat{a}. \tag{52}$$

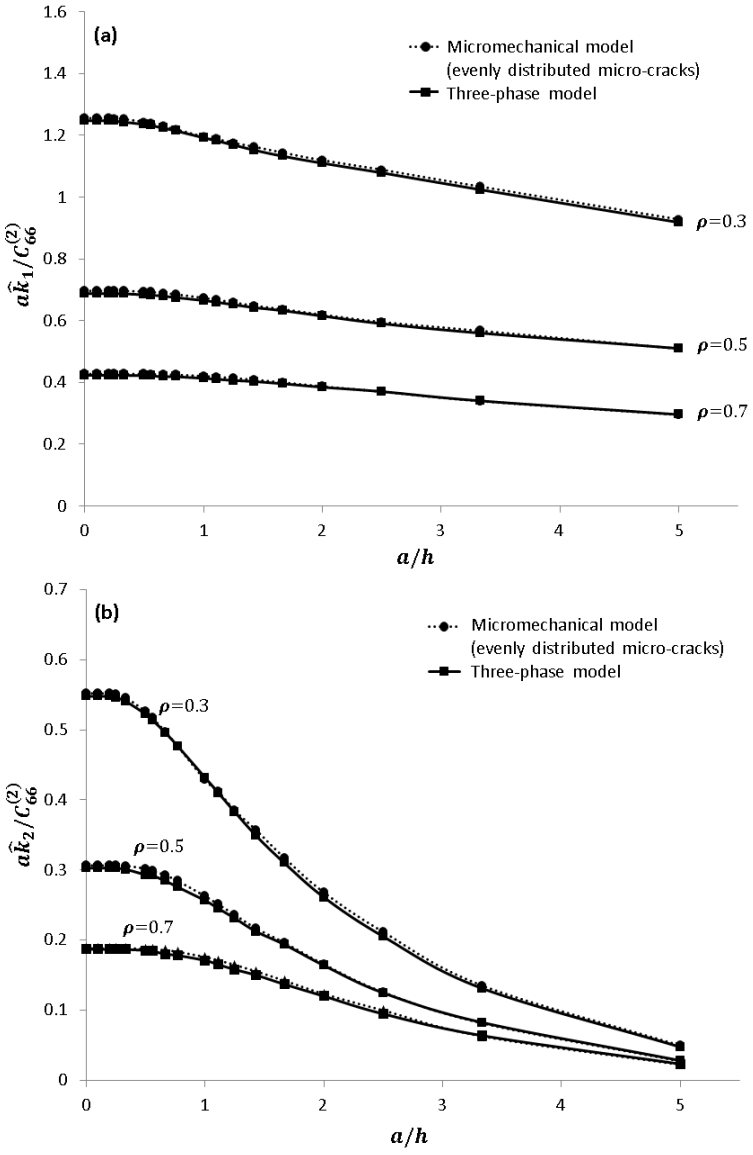

Figure 3. A graphic comparison of $a\widehat{k}_1/C_{66}^{(2)}$ and $a\widehat{k}_2/C_{66}^{(2)}$ calculated by using the micromechanical model in Section 4 (with evenly distributed equal length micro-cracks) and the three-phase model.

For fixed values of ρ and $\widehat{a}/h$ (h is the thickness of the elastic layer), N interfaces are randomly generated to form a sample for generating statistical data for the effective stiffness coefficients $\widehat{k}_1$ and $\widehat{k}_2$.

6.1 Number of micro-cracks for homogenizing the interface

The number of micro-cracks required per period interval of the interface for homogenizing the effective stiffness coefficients is investigated here by randomly generating 50 micro-cracked interfaces for fixed values of ρ and $\widehat{a}/h$. The M micro-crack lengths follow a χ^2 distribution of a fixed degree of freedom k, that is, the $\chi^2(k)$ distribution. For each of the interfaces, the non-dimensionalized effective stiffness coefficients $\widehat{a}\widehat{k}_1/C_{66}^{(2)}$ and $\widehat{a}\widehat{k}_2/C_{66}^{(2)}$ are calculated as explained in Subsection 4.4. The mean values of $\widehat{a}\widehat{k}_1/C_{66}^{(2)}$ and $\widehat{a}\widehat{k}_2/C_{66}^{(2)}$ from the 50 interfaces should not vary much when M exceeds a certain value M_0, which is taken to be the number of micro-cracks required for homogenizing the interface. The elastic moduli for graphite-epoxy and E-glass-expoxy given in Table 1 in Section 5 are used here for the material constants of the orthotropic thin layer and the orthotropic half-space respectively.

For $\rho = 0.5$ and $\widehat{a}/h = 1$, Figure 4 gives the scatter plots of the data for non-dimensionalized effective stiffness coefficients $\widehat{a}\widehat{k}_1/C_{66}^{(2)}$ and $\widehat{a}\widehat{k}_2/C_{66}^{(2)}$ of the 50 interfaces against various values of M. The means of $\widehat{a}\widehat{k}_1/C_{66}^{(2)}$ and $\widehat{a}\widehat{k}_2/C_{66}^{(2)}$ are also indicated in Figure 4 for the different values of M. It is observed that both the mean values of $\widehat{a}\widehat{k}_1/C_{66}^{(2)}$ and $\widehat{a}\widehat{k}_2/C_{66}^{(2)}$ decrease drastically as M increases from 10 to 40. When M exceeds 40, the mean values of $\widehat{a}\widehat{k}_1/C_{66}^{(2)}$ and $\widehat{a}\widehat{k}_2/C_{66}^{(2)}$ do not change very much. Moreover, as M increases from 40 to 60, the ranges over which the data of $\widehat{a}\widehat{k}_1/C_{66}^{(2)}$ and $\widehat{a}\widehat{k}_2/C_{66}^{(2)}$ scat-

ter are more or less the same and are narrower than the scattering ranges for M between 10 and 40. It appears that 40 micro-cracks per period interval of the interface may be sufficient for homogenizing the non-dimensionalized effective stiffness coefficients. Similar observations apply for various other values of ρ and $\widehat{a}/h$ and for micro-cracks generated using a χ^2 distribution of a different degree of freedom.

6.2 Influence of the micro-crack length distribution

The influence of the micro-crack length distribution on the mean value of the non-dimensionalized effective stiffness coefficients $\widehat{a}\widehat{k}_1/C_{66}^{(2)}$ and $\widehat{a}\widehat{k}_2/C_{66}^{(2)}$ is investigated here. For fixed values of ρ and $\widehat{a}/h$, a sample of 50 randomly generated micro-cracked interfaces is used for the statistical simulation of the interface. As suggested by the analysis in Subsection 6.1, the number of micro-cracks over a period interval of the interface is taken to be 40. For each interface, the micro-crack length follows the $\chi^2(k)$ distribution. To examine how the mean values of $\widehat{a}\widehat{k}_1/C_{66}^{(2)}$ and $\widehat{a}\widehat{k}_2/C_{66}^{(2)}$ may be affected by different values of k (that is, by different micro-crack length distributions), the micro-cracks are positioned in such a way that the crack-tip gap g between two adjacent micro-cracks is a constant given by $g = 2\widehat{a}(1-\rho)/\rho$. As in the simulations in Subsection 6.1, the materials in the thin layer and the half-space are selected to be graphite-epoxy and E-glass-expoxy respectively with the elastic moduli given in Table 1.

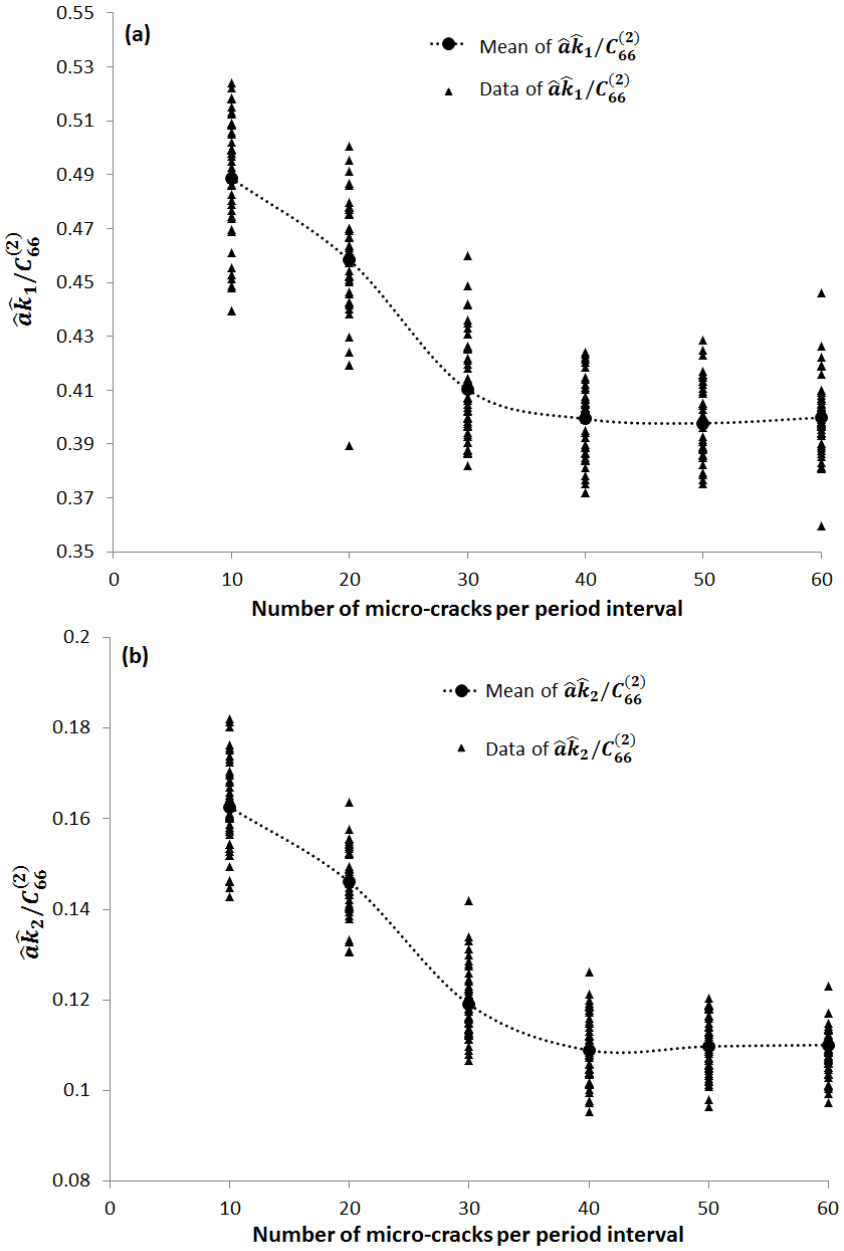

Figure 4. Scatter plots and mean values of the non-dimensionalized effective stiffness $\widehat{a}\widehat{k}_1/C_{66}^{(2)}$ and $\widehat{a}\widehat{k}_1/C_{66}^{(2)}$ against M.

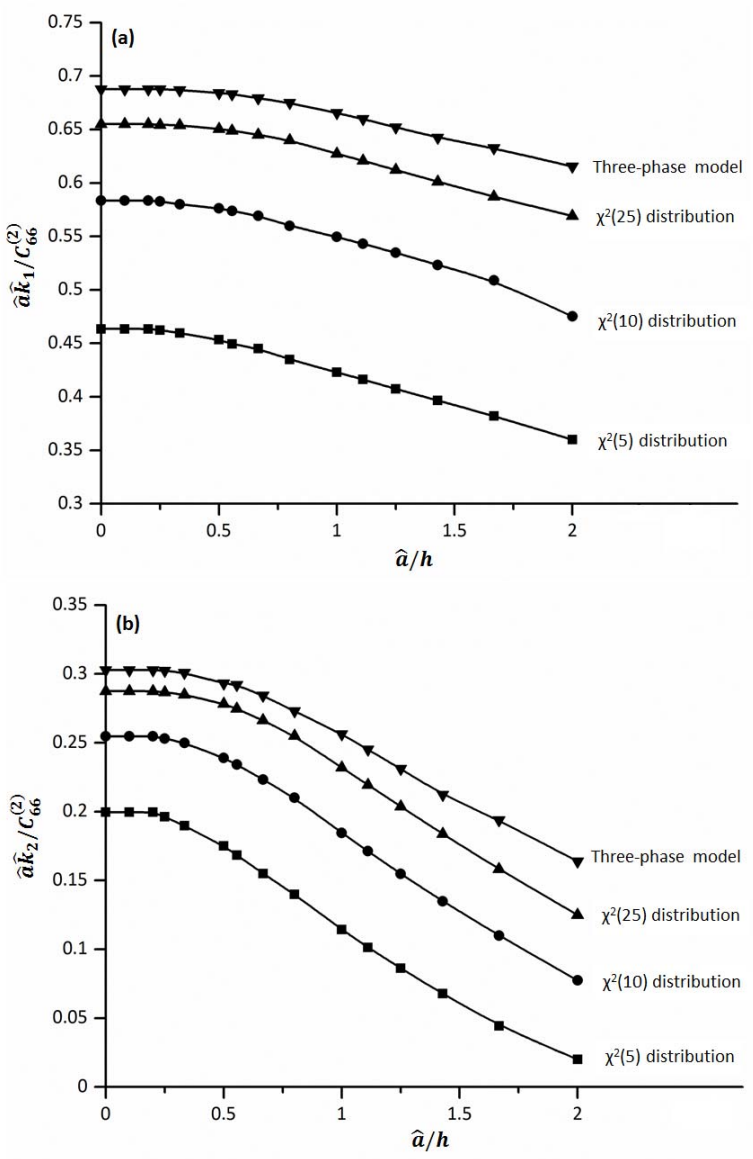

Figure 5. Plots of $\widehat{a}\widehat{k}_1/C_{66}^{(2)}$ and $\widehat{a}\widehat{k}_2/C_{66}^{(2)}$ against $\widehat{a}/h$ for $\rho = 0.5$ and cases where the micro-crack length follows the $\chi^2(5)$, $\chi^2(10)$ and $\chi^2(25)$ distributions. Also given are plots of the corresponding non-dimensionalized stiffness coefficients computed by using the three-phase model.

For $\rho = 0.5$, the mean values of $\widehat{a}\widehat{k}_1/C_{66}^{(2)}$ and $\widehat{a}\widehat{k}_2/C_{66}^{(2)}$ against $\widehat{a}/h$ are plotted in Figure 5 for cases where the $\chi^2(5)$, $\chi^2(10)$ and $\chi^2(25)$ distribution are used for generating the lengths of the micro-cracks. Plots of the corresponding non-dimensionalized effective stiffness coefficients predicted by the three-phase model are also given in Figure 5. From Figure 5, it is obvious that the mean values of the effective stiffness coefficients are influenced by the random micro-crack length distribution. It is also observed that $\widehat{a}\widehat{k}_1/C_{66}^{(2)}$ and $\widehat{a}\widehat{k}_2/C_{66}^{(2)}$ become closer to the corresponding values predicted by the three-phase model, as the micro-crack length distribution becomes more normal-like, that is, the degree of freedom k of the χ^2 distributions increases. This observation is not surprising for the following reason. The ratio of the standard deviation of the $\chi^2(k)$ distribution to the mean of the distribution is given by $\sqrt{2/k}$. This ratio tends to zero as k increases, that is, the variation in the micro-crack length (relative to the mean of the micro-crack length) decreases as k increases. Thus, for a very large value of k, the micro-cracks may be regarded to be of equal length and evenly distributed on the interface. As observed in Section 5, the three-phase model agrees more closely with the micromechanical model when the micro-cracks are of equal length and are evenly distributed.

6.3 Case studies using specific orthotropic materials

The micromechanical-statistical model is used here to simulate the micro-cracked interface between a selected pair of dissimilar orthotropic materials.

As before, for selected values of ρ and $\widehat{a}/h$, 50 micro-cracked interfaces are randomly generated for the statistical simulations. For each interface, 40 micro-cracks are randomly chosen with their lengths following the $\chi^2(5)$

distribution. The micro-cracks are positioned randomly over a period interval of the interface.

The elastic moduli (in GPa) for boron-epoxy as given in Table 1 are used as the material constants for the elastic half-space. Three different orthotropic materials of differing strength, namely carbon-epoxy, graphite-epoxy and martensite, with elastic moduli as given in Table 1, are selected in turn to be the material in the thin layer.

Table 1. Elastic moduli (in GPa) for selected orthotropic materials.

	C_{11}	C_{22}	C_{12}	C_{66}
Boron-epoxy	209.1	20.0	5.1	6.4
Carbon-epoxy	136.2	9.2	3.9	4.3
E-glass-epoxy	46.1	12.6	2.9	5.5
Graphite-epoxy	155.4	16.3	3.7	7.5
Martensite	233.0	233.0	135.0	118.0

For $\rho = 0.5$, the mean values of $\widehat{a}\widehat{k}_1/C_{66}^{(2)}$ and $\widehat{a}\widehat{k}_2/C_{66}^{(2)}$ against $\widehat{a}/h$ are plotted in Figure 6 for the cases where carbon-epoxy, graphite-epoxy and martensite are used as the material in the thin layer. For a fixed $\widehat{a}/h$, the interface for the case where the thin layer is occupied by martensite has the largest effective stiffness coefficients $\widehat{a}\widehat{k}_1/C_{66}^{(2)}$ and $\widehat{a}\widehat{k}_2/C_{66}^{(2)}$, while the values of $\widehat{a}\widehat{k}_1/C_{66}^{(2)}$ and $\widehat{a}\widehat{k}_2/C_{66}^{(2)}$ are the smallest for the case where the thin layer is carbon-epoxy. Thus, the effective stiffness coefficients of the interface appear to be larger in magnitude if the material of the thin layer has larger elastic moduli. This observation is consistent with our intuition that coating a layer of "stronger" material on the half-space may reduce the magnitudes of the displacement jumps over the micro-cracks to give rise to larger effective stiffness coefficients. Note that the effective stiffness coefficients are calculated using the average displacement jumps over the micro-cracks.

Each of the plots in Figure 6 shows that the mean values of $\widehat{a}\widehat{k}_1/C_{66}^{(2)}$ and $\widehat{a}\widehat{k}_2/C_{66}^{(2)}$ decrease as $\widehat{a}/h$ increases. As explained in Section 5, as $\widehat{a}/h$ increases, that is, as the thickness of the layer becomes smaller compared to the average length of the micro-cracks, the edge of the layer has the effect of increasing the magnitudes of the displacement jumps across the micro-cracks, thereby reducing the effective stiffness coefficients of the interface.

6.4 Isotropic elastic layer and half-space

The case where the elastic layer and the elastic half-space are both isotropic is considered here. For isotropic materials, the elastic moduli are given by

$$C_{11}^{(p)} = C_{22}^{(p)} = \lambda^{(p)} + 2\mu^{(p)},\ C_{66}^{(p)} = \mu^{(p)} \text{ and } C_{12}^{(p)} = \lambda^{(p)}, \tag{53}$$

where $\lambda^{(p)}$ and $\mu^{(p)}$ are the Lamé constants of the isotropic materials.

The analysis given in the earlier sections for general orthotropic materials appears to break down for isotropic materials, as constants such as $N_{\alpha k}^{(p)}$ and $M_{\alpha k}^{(p)}$ are ill-defined if the elastic moduli are given by (53). Nevertheless, it may be recovered for isotropic materials by using a limiting procedure given in Ang [1]. More specifically, the hypersingular integral and integro-differential equations for the micromechanical-statistical model can be recovered for isotropic materials by replacing $C_{12}^{(p)} = \lambda^{(p)}$ in (53) with $C_{12}^{(p)} = \lambda^{(p)}(1-\varepsilon)$ and letting the real parameter ε tend to zero.

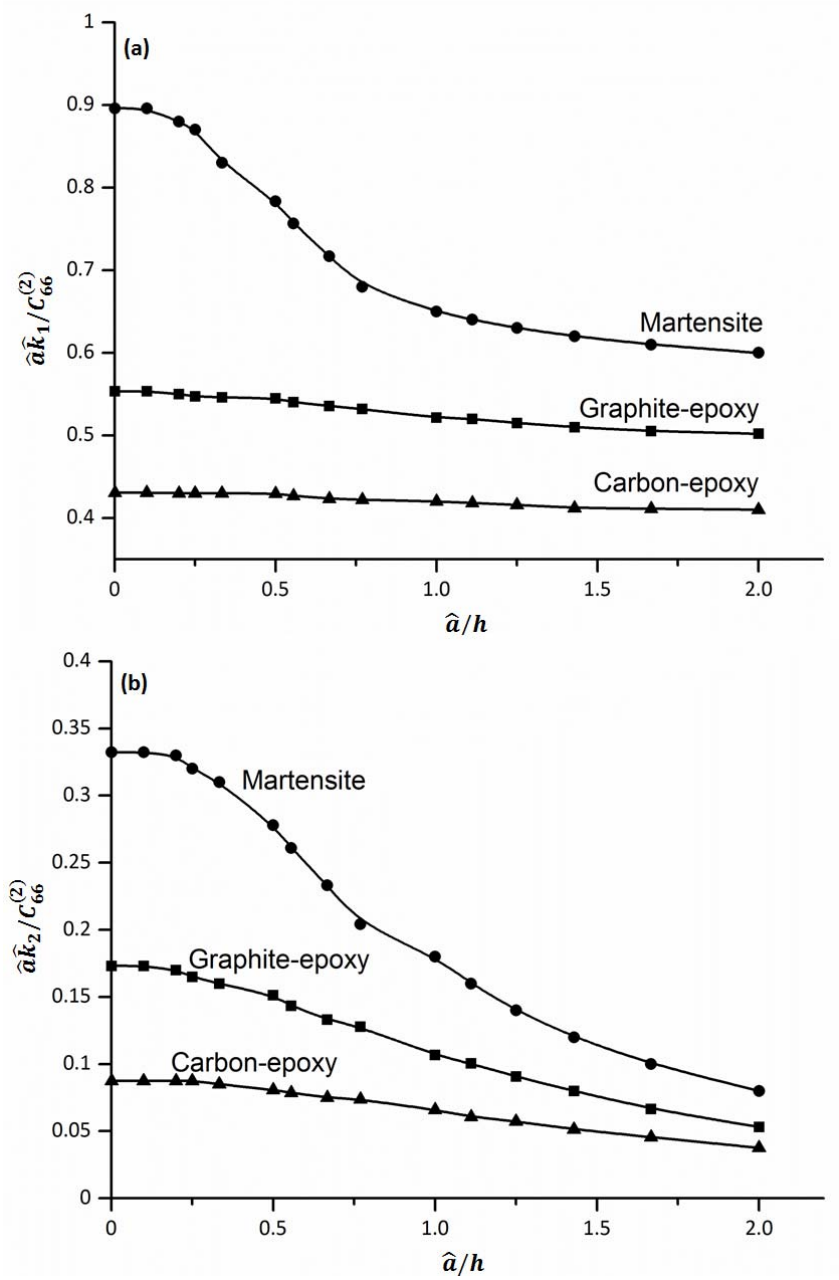

Figure 6. Plots of $\widehat{a}\widehat{k}_1/C_{66}^{(2)}$ and $\widehat{a}\widehat{k}_2/C_{66}^{(2)}$ against $\widehat{a}/h$ for selected thin layer materials.

For isotropic materials, the hypersingular integral and integro-differential equations in (48) and (49) reduce to

$$\begin{aligned}
&\frac{1}{2\pi}\oint_0^L \frac{1}{\gamma}u_r^{(\mathrm{imp})}(x_1,h)\widetilde{G}_{ri}[\frac{1}{(x_1-\xi_1)^2}+\Theta(x_1,\xi_1)]dx_1\\
&+\frac{1}{2\pi}\int_0^L \frac{1}{\gamma}u_r^{(\mathrm{imp})}(x_1,h)\,\mathrm{Re}\{\widetilde{H}_{ri}\Omega(x_1,\xi_1,2ih)\}dx_1\\
&-\frac{1}{2\pi}\sum_{k=1}^{M}\int_{a^{(k)}}^{b^{(k)}} \frac{1}{\gamma}\Delta u_r^{(\mathrm{imp})}(x_1)\,\mathrm{Re}\{\widetilde{G}_{ri}\Omega(x_1,\xi_1,-ih)\}dx_1\\
&-\frac{1}{2\pi}\sum_{k=1}^{M}\int_{a^{(k)}}^{b^{(k)}} \frac{1}{\gamma}\Delta u_r^{(\mathrm{imp})}(x_1)\,\mathrm{Re}\{\widetilde{H}_{ri}\Omega(x_1,\xi_1,ih)\}dx_1\\
=\;& 0 \;\text{ for } 0<\xi_1<L, \qquad (54)
\end{aligned}$$

and

$$\begin{aligned}
&-\frac{1}{2\pi}\int_0^L \frac{1}{\gamma}u_r^{(\mathrm{imp})}(x_1,h)\,\mathrm{Re}\{\Omega(x_1,\xi_1,ih)(\widetilde{G}_{ri}+\widetilde{H}_{ri})\}dx_1\\
&+\frac{1}{2\pi}[\oint_{a^{(k)}}^{b^{(k)}} \frac{\Delta u_r^{(\mathrm{imp})}(x_1)\widetilde{W}_{ri}}{\gamma(x_1-\xi_1)^2}dx_1\\
&+\sum_{\substack{n=1\\ n\neq k}}^{M}\int_{a^{(n)}}^{b^{(n)}} \frac{\Delta u_r^{(\mathrm{imp})}(x_1)\widetilde{W}_{ri}}{\gamma(x_1-\xi_1)^2}dx_1\\
&+\sum_{n=1}^{M}\int_{a^{(n)}}^{b^{(n)}} \frac{1}{\gamma}\Delta u_r^{(\mathrm{imp})}(x_1)\widetilde{W}_{ri}\Theta(x_1,\xi_1)dx_1-\frac{\pi\widetilde{V}_{ri}}{\gamma}\frac{d(\Delta u_r^{(\mathrm{imp})}(\xi_1))}{d\xi_1}]\\
=\;& \delta_{i1}S+\delta_{i2}T \;\text{ for } a^{(k)}<\xi_1<b^{(k)}\ (k=1,2,...,M), \qquad (55)
\end{aligned}$$

where

$$
\begin{aligned}
[\widetilde{G}_{ri}] &= \begin{bmatrix} -\dfrac{4}{1+\alpha} & 0 \\ 0 & -\dfrac{4}{1+\alpha} \end{bmatrix}, \\
[\widetilde{H}_{ri}] &= \begin{bmatrix} -\dfrac{4}{1-\beta^2}+\dfrac{4}{1+\alpha} & \dfrac{4\beta}{1-\beta^2}i \\ -\dfrac{4\beta}{1-\beta^2}i & -\dfrac{4}{1-\beta^2}+\dfrac{4}{1+\alpha} \end{bmatrix}, \\
[\widetilde{W}_{ri}] &= \begin{bmatrix} -\dfrac{4}{1-\beta^2} & 0 \\ 0 & -\dfrac{4}{1-\beta^2} \end{bmatrix}, \\
[\widetilde{V}_{ri}] &= \begin{bmatrix} 0 & \dfrac{4\beta}{1-\beta^2} \\ -\dfrac{4\beta}{1-\beta^2} & 0 \end{bmatrix}, \qquad (56)
\end{aligned}
$$

and α, β and γ are defined by

$$
\begin{aligned}
\alpha &= \frac{1}{\gamma}\left(\frac{\lambda^{(1)}+2\mu^{(1)}}{\mu^{(1)}(\lambda^{(1)}+\mu^{(1)})} - \frac{\lambda^{(2)}+2\mu^{(2)}}{\mu^{(2)}(\lambda^{(2)}+\mu^{(2)})}\right), \\
\beta &= \frac{1}{\gamma}\left(\frac{1}{\lambda^{(1)}+\mu^{(1)}} - \frac{1}{\lambda^{(2)}+\mu^{(2)}}\right), \\
\gamma &= \frac{\lambda^{(1)}+2\mu^{(1)}}{\mu^{(1)}(\lambda^{(1)}+\mu^{(1)})} + \frac{\lambda^{(2)}+2\mu^{(2)}}{\mu^{(2)}(\lambda^{(2)}+\mu^{(2)})}. \qquad (57)
\end{aligned}
$$

In the literature, the non-dimensionalized constants α and β are known as the Dundurs' parameters (see, for example, Schmauder [18] and Schmauder and Meyer [19]).

For the special case where $a/h \to 0^+$, (55) reduces to

$$\begin{aligned}
&\frac{1}{2\pi}[\neq\int_{a^{(k)}}^{b^{(k)}} \frac{\Delta u_r^{(\mathrm{imp})}(x_1)\widetilde{W}_{ri}}{\gamma(x_1-\xi_1)^2}dx_1 \\
&+\sum_{\substack{n=1\\n\neq k}}^{M}\int_{a^{(n)}}^{b^{(n)}} \frac{\Delta u_r^{(\mathrm{imp})}(x_1)\widetilde{W}_{ri}}{\gamma(x_1-\xi_1)^2}dx_1 \\
&+\sum_{n=1}^{M}\int_{a^{(n)}}^{b^{(n)}} \frac{1}{\gamma}\Delta u_r^{(\mathrm{imp})}(x_1)\widetilde{W}_{ri}\Theta(x_1,\xi_1)dx_1 - \frac{\pi\widetilde{V}_{ri}}{\gamma}\frac{d(\Delta u_r^{(\mathrm{imp})}(\xi_1))}{d\xi_1}] \\
= \;& \delta_{i1}S+\delta_{i2}T \text{ for } a^{(k)}<\xi_1<b^{(k)} \ (k=1,2,...,M). \qquad (58)
\end{aligned}$$

Thus, for the special case where the interface lies between two isotropic elastic half-spaces, the effective stiffness coefficients of the interface may be computed using (44) after solving the hypersingular integro-differential equations in (58).

To perform micromechanical-statistical simulations to estimate the non-dimensionalized effective stiffness coefficients $\gamma\widehat{a}\widehat{k}_1$ and $\gamma\widehat{a}\widehat{k}_2$ of the interface for given values α, β, ρ and $\widehat{a}/h$, 50 micro-cracked interfaces are randomly generated. For each interface, the $\chi^2(5)$ distribution is used to randomly generate the 40 micro-cracks which are then randomly located over a period interval of the interface. Note that $\widehat{a}$ is the average half-length of the 40 micro-cracks.

For a given interface between two isotropic half-spaces (that is, for the case where $\widehat{a}/h \to 0^+$), $\gamma\widehat{a}\widehat{k}_1$ and $\gamma\widehat{a}\widehat{k}_2$ vary with only the Dundurs' parameter β. This is obvious from the hypersingular integro-differential equations (58), if we note that $\widetilde{W}_{ri}$ and $\widetilde{V}_{ri}$ depend on β only. Also, note that $\widehat{k}_1 = \widehat{k}_2$ here. The mean values of $\gamma\widehat{a}\widehat{k}_1$ computed from the sample of 50 randomly generated micro-cracked interfaces are computed and plotted against β for $\beta \geq 0$ in Figure 7 for selected values of ρ. For $\beta \geq 0$, the mean value of $\gamma\widehat{a}\widehat{k}_1$ increases as β increases. Note that $\gamma\widehat{a}\widehat{k}_1$ here is an even function of β, since

the effective stiffness coefficients $\widehat{k}_1$ and $\widehat{k}_2$ remain the same if the materials in the two half-spaces are interchanged.

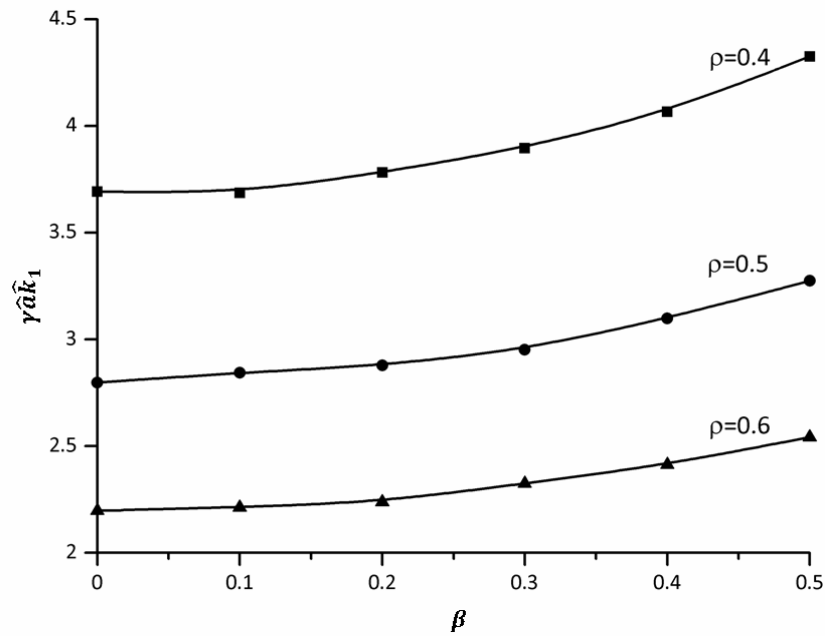

Figure 7. Plots of $\gamma\widehat{a}\widehat{k}_1$ against β for selected values of ρ.

The Dundurs' parameters α and β and the parameter γ in (57) may rewritten in terms of the Young's moduli $E^{(1)}$ and $E^{(2)}$and the Poisson's ratios $\nu^{(1)}$ and $\nu^{(2)}$ (of the thin elastic layer and the elastic half-space) as

(Schmauder and Meyer [19])

$$\begin{aligned}
\alpha &= \frac{\dfrac{E^{(2)}}{E^{(1)}} - \dfrac{(1-\nu^{(2)})(1+\nu^{(2)})}{(1-\nu^{(1)})(1+\nu^{(1)})}}{\dfrac{E^{(2)}}{E^{(1)}} + \dfrac{(1-\nu^{(2)})(1+\nu^{(2)})}{(1-\nu^{(1)})(1+\nu^{(1)})}}, \\
\beta &= \frac{1}{2}\frac{\dfrac{E^{(2)}}{E^{(1)}}(1-2\nu^{(1)})(1+\nu^{(1)}) - (1-2\nu^{(2)})(1+\nu^{(2)})}{\dfrac{E^{(2)}}{E^{(1)}}(1-\nu^{(1)})(1+\nu^{(1)}) + (1-\nu^{(2)})(1+\nu^{(2)})}, \\
\gamma &= \frac{4}{E^{(2)}}[\frac{E^{(2)}}{E^{(1)}}(1-\nu^{(1)})(1+\nu^{(1)}) + (1-\nu^{(2)})(1+\nu^{(2)})]. \qquad (59)
\end{aligned}$$

For a particular case study, we take $\nu^{(1)} = \nu^{(2)} = \nu$ and examine how $E^{(1)}/E^{(2)}$ and ν may affect the non-dimensionalized effective stiffness coefficients $\widehat{a}\widehat{k}_1/E^{(2)}$ and $\widehat{a}\widehat{k}_2/E^{(2)}$. For selected $E^{(1)}/E^{(2)}$, ν, ρ and $\widehat{a}/h$, a sample of 50 interfaces are randomly generated. Each interface contains 40 micro-cracks that are randomly positioned over a period interval of the interface. The micro-crack length follows the $\chi^2(5)$ distribution.

For $\rho = 0.5$ and $\nu = 0.25$, plots of the non-dimensionalized effective stiffness coefficients $\widehat{a}\widehat{k}_1/E^{(2)}$ and $\widehat{a}\widehat{k}_2/E^{(2)}$ against $\log_{10}(E^{(1)}/E^{(2)})$ for selected values of $\widehat{a}/h$ in Figure 8. For moderate values of $E^{(1)}/E^{(2)}$ within the range $-0.5 < \log_{10}(E^{(1)}/E^{(2)}) < 2$, the plots for various $\widehat{a}/h$ are visually distinguishable and it is obvious that both $\widehat{a}\widehat{k}_1/E^{(2)}$ and $\widehat{a}\widehat{k}_2/E^{(2)}$ increases with the increasing $\log_{10}(E^{(1)}/E^{(2)})$ for a fixed $\widehat{a}/h$. For $E^{(1)}/E^{(2)}$ larger than 100, all the plots of $\widehat{a}\widehat{k}_1/E^{(2)}$ and $\widehat{a}\widehat{k}_2/E^{(2)}$ in Figure 8 tend to the same constant, approximately 0.81, as $E^{(1)}/E^{(2)}$ increases. It appears that the effect of the edge of the thin layer becomes negligible if the thin layer can be made sufficiently strong compared to the elastic half-space. Both $\widehat{a}\widehat{k}_1/E^{(2)}$ and $\widehat{a}\widehat{k}_2/E^{(2)}$ tend to zero as $E^{(1)}/E^{(2)}$ tends to zero for the selected values of $\widehat{a}/h$.

For a selected value of $\log_{10}(E^{(1)}/E^{(2)})$, we observe that the mean values

of $\widehat{a}\widehat{k}_1/E^{(2)}$ increase less than values of $\widehat{a}\widehat{k}_2/E^{(2)}$ as $\widehat{a}/h$ decreases from 2 to 0. This seems to suggest that varying the thickness of the layer has a more significant effect on the average value of x_2 component of the crack opening displacement compared to the average value of the x_1 component.

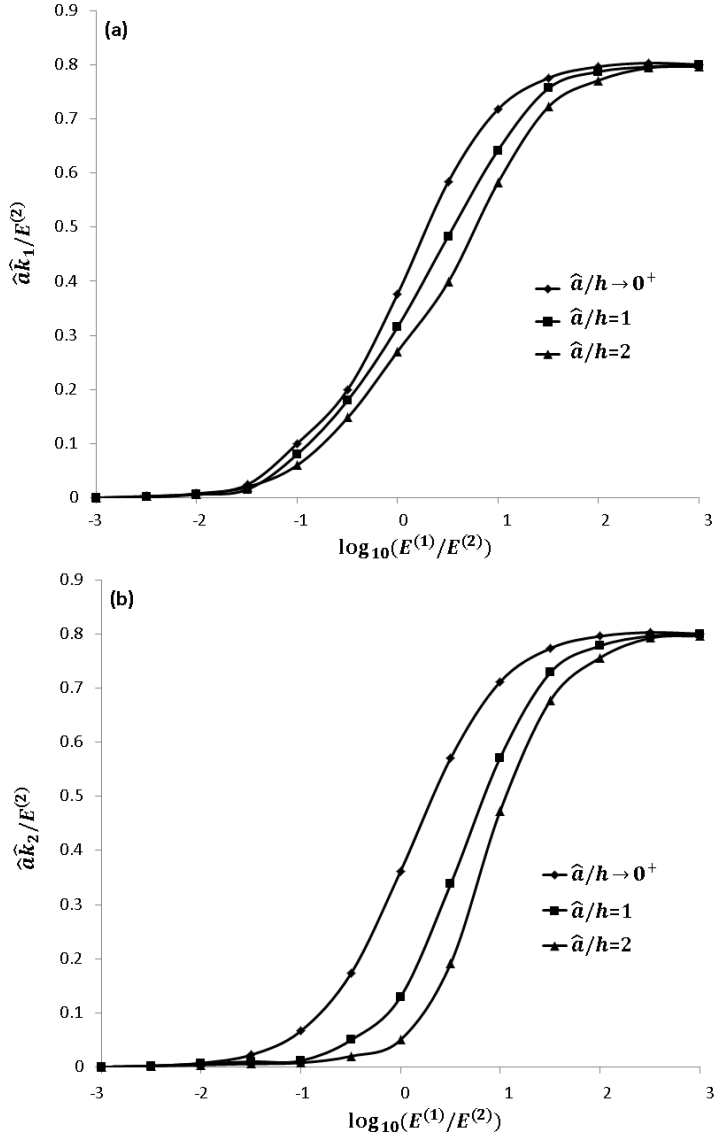

Figure 8. Plots of the non-dimensionalized effective stiffness $\widehat{a}\widehat{k}_1/E^{(2)}$ and $\widehat{a}\widehat{k}_2/E^{(2)}$ against $\log_{10}(E^{(1)}/E^{(2)})$ for selected values of $\widehat{a}/h$.

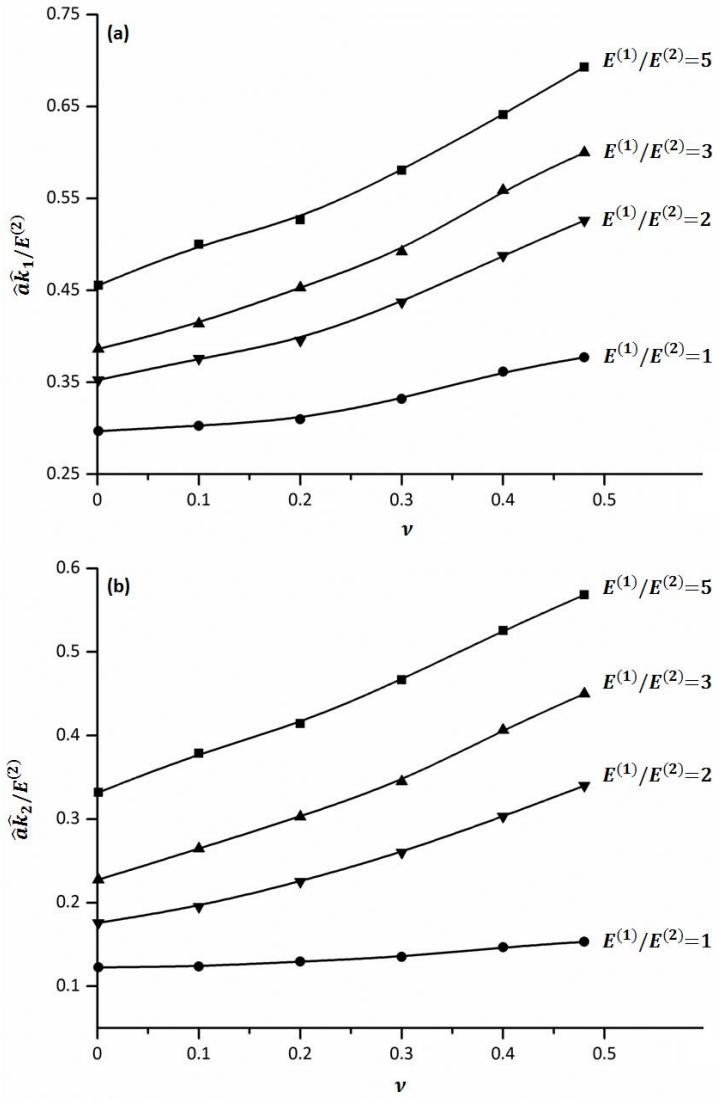

Figure 9. Plots of $\widehat{a}\widehat{k}_1/E^{(2)}$ and $\widehat{a}\widehat{k}_2/E^{(2)}$ against ν for selected values of $E^{(1)}/E^{(2)}$

For $\rho = 0.5$ and $\widehat{a}/h = 1$, plots of the non-dimensionalized effective

stiffness coefficients $\widehat{a}\widehat{k}_1/E^{(2)}$ and $\widehat{a}\widehat{k}_2/E^{(2)}$ against ν are given in Figure 9 for selected values of $E^{(1)}/E^{(2)}$. For a fixed $E^{(1)}/E^{(2)}$, both $\widehat{a}\widehat{k}_1/E^{(2)}$ and $\widehat{a}\widehat{k}_2/E^{(2)}$ increase as ν increases from 0 to 0.5. It appears that the effective stiffness coefficients of the interface increase as the isotropic materials in the elastic layer and the elastic half-space becomes more incompressible.

7 Summary and conclusions

The present paper extends the work in Wang *et al* [21] to the micromechanical analysis of a microscopically damaged interface between an orthotropic thin elastic layer and a dissimilar orthotropic elastic half-space under inplane deformations. Two micromechanical models based on the hypersingular integral and integro-differential equations are proposed to estimate the effective stiffness coefficients of the damaged interface which is modeled as containing periodic arrays of micro-cracks. The first model, known as the three-phase model, simplifies each period of the micro-cracked interface into three parts – a representative micro-crack, an effective region and perfectly bonded regions. The second model − the micromechanical-statistical model − simulate a period interval of the damaged interface as containing an arbitrary number of randomly positioned micro-cracks with lengths that are randomly generated to follow a selected χ^2 distribution. Both models are formulated and numerically solved in terms of hypersingular integral and integro-differential equations.

As a check, the effective stiffness coefficients estimated by the three-phase model for a particular pair of orthotropic materials are compared with those calculated from the micromechanical model in Section 4 with all micro-cracks having equal length and being evenly distributed along the interface. As expected, the values of the effective stiffness coefficients given by the two models

are in close agreement, especially when the damage ratio of the interface is not too close to unity. For $0.1 \leq \rho \leq 0.9$ and $0 < a/h \leq 5$, the maximum percentage difference between the effective stiffness coefficients computed using the three-phase model and those by the micromechanical model is between 0.012% and 5.5%.

Statistical simulations conducted on the micro-cracked interface suggest least 40 micro-cracks are required in the micromechanical-statistical model to homogenize the effective stiffness coefficients of the interface. Furthermore, the simulations show that the effective stiffness coefficients are significantly influenced by the degree of freedom of the χ^2 distribution used to generate the lengths of the micro-cracks. As the degree of freedom increases, that is, as the variation of the micro-crack length compared to the average micro-crack length becomes smaller, the effective stiffness coefficients are closer to those predicted by the three-phase model. The three-phase model overestimates the values of the effective stiffness coefficients.

Two specific case studies involving particular materials in the layer and the half-space are conducted by using the micromechanical-statistical model.

In the first case study, the effective stiffness coefficients of the interface are calculated for three different particular orthotropic materials in the layer. As expected, the effective stiffness coefficients are larger when the orthotropic material in the layer is "stronger". For a given interface between a given pair of materials, the effective stiffness coefficients increase as $\widehat{a}/h$ decreases.

In the second case study, the elastic materials in the thin layer and the half-space are taken to be isotropic. For isotropic materials, the coefficients in the hypersingular integral and integro-differential equations for the micromechanical-statistical model are expressed in terms of the Dundurs' parameters α and β. The coefficients are found to be independent of α if the

isotropic elastic layer is replaced by an isotropic elastic half-space. Statistical simulations conducted for the case where the materials in the layer and the half-space have the same Poisson's ratio show that the effect of the thin edge of the layer on the effective stiffness coefficients of the interface may be made negligible by increasing the Young's modulus of the material in the layer. Furthermore, the effective stiffness coefficients of the interface are observed to increase as the materials in the layer and the half-space become more incompressible.

References

[1] W. T. Ang, *Hypersingular Integral Equations in Fracture Analysis,* Woodhead Publishing, Cambridge, 2013.

[2] J. R. Berger and V. K. Tewary, Green's functions for boundary element analysis of anisotropic bimaterials, *Engineering Analysis with Boundary Elements* **25** (2001) 279-288.

[3] E. L. Chen and W. T. Ang, Green's functions and boundary element analysis for bimaterials with soft and stiff planar interfaces under plane elastostatic deformations, *Engineering Analysis with Boundary Elements* **40** (2014) 50-61.

[4] J. T. Chen and H.-K. Hong, Review of dual boundary element methods with emphasis on hypersingular integrals and divergent series, *ASME Applied Mechanics Reviews* **52** (1999) 17-33.

[5] R. M. Christensen and K. H. Lo, Solutions for effective shear properties in three phase sphere and cylinder models, *Journal of the Mechanics and Physics of Solids* **27** (1979) 315-330.

[6] D. L. Clements, *Boundary Value Problems Governed by Second Order Elliptic Systems*, Pitman, London, 1981.

[7] J. D. Eshelby, W. T. Read and W. Shockley, Anisotropic elasticity with application to dislocation theory, *Acta Metallurgica* **1** (1953) 251-259.

[8] H. Fan and K. Y. Sze, A micro-mechanics model for imperfect interface in dielectric materials, *Mechanics of Materials* **33** (2001) 363-370.

[9] S. Glodež, N. Jezernik, J. Kramberger and T. Lassen, Numerical modelling of fatigue crack initiation of martensitic steel, *Advances in Engineering Software* **41** (2010) 823–829.

[10] A. Guechaichia and I. Trendafilova, A simple frequency-based delamination detection and localization method without baseline model, *Journal of Physics: Conference Series* **382** (2012) 012033.

[11] Z. Hashin, The spherical inclusion with imperfect interface, *ASME Journal of Applied Mechanics* **58** (1991) 444-449.

[12] H.-K. Hong and J. T. Chen, Derivations of integral equations of elasticity, *ASCE Journal of Engineering Mechanics* **114** (1988) 1028-1044.

[13] J. P. Jones and J. S. Whittier, Waves at a flexibly bonded interface, *Journal of Applied Mechanics* **34** (1967) 905-909.

[14] A. C. Kaya and F. Erdogan, On the solution of integral equations with strongly singular kernels, *Quarterly of Applied Mathematics* **45** (1987) 105-122.

[15] P. A. Martin, Thin interface layers: adhesives, approximations and analysis, in *Elastic Waves and Ultrasonic Nondestructive Evaluation*, 217–222, edited by S. K. Datta, J. D. Achenbach, and Y. S. Rajapakse, North-Holland, Amsterdam, 1990.

[16] F. J. Rizzo, An integral equation approach to boundary value problems of classical elastostatics, *Quarterly of Applied Mathematics* **25** (1967) 83-95.

[17] C. Rubio-Gonzalez and J. J. Mason, Dynamic stress intensity factors at the tip of a uniformly loaded semi-infinite crack in an orthotropic material, *Journal of the Mechanics and Physics of Solids* **48** (2000) 899-925.

[18] S. Schmauder, Interfacial fracture in the presence of residual stresses, *Fracture Mechanics of Ceramics* **12** (1996) 443-450.

[19] S. Schmauder and M. Meyer, Correlation between Dundurs' parameters and elastic constants, *Z. Metallkd.* **83** (1992) 524-527.

[20] L. J. Sudak and X. Wang, Green's function in plane anisotropic bimaterials with imperfect interface, *IMA Journal of Applied Mathematics* **71** (2006) 783-794.

[21] X. Wang, W. T. Ang and H. Fan, Micro-mechanics models for an imperfect interface under anti-plane shear load: Hypersingular integral formulations, *Engineering analysis with Boundary Elements* **36** (2012) 1856-1864.

[22] X. Wang, H. Fan and W. T. Ang, On micromechanical-statistical modeling of microscopically damaged interfaces under antiplane deformations, *International Journal of Solids and Structures* **51** (2014) 2327-2335.